

Particle Fluxes in Atomic Collision Cascades

By M. W. Sckerl, P. Sigmund *and* M. Vicanek



Matematisk-fysiske Meddelelser **44:3**

Det Kongelige Danske Videnskabernes Selskab
The Royal Danish Academy of Sciences and Letters

Commissioner: Munksgaard · Copenhagen 1996

Synopsis

The flux of recoil atoms in atomic collision cascades induced by an ion beam or another source of energetic particles in a material is known to approach isotropy at kinetic energies far below the beam energy. A variety of irradiation effects can be explained satisfactorily on the basis of an isotropic particle flux, but significant deviations from this simple behavior are known to exist. While numerous examples have been studied by numerical simulation of cascade processes, the systematics is, by and large, unknown. The present study aims at general scaling properties and estimates of the magnitude of moderate deviations from isotropy and their spatial dependence for a wide range of beam and material parameters. Anisotropies introduced by crystal structure are ignored.

Although it is well established that cascade anisotropy is related to the momentum of beam particles, previous attempts to quantify this relation have failed. We have found that there are two leading correction terms to the isotropic particle flux, a well-known term centered around the beam direction as a symmetry axis and a new term proportional to the gradient of the deposited-energy density. As a general rule the two contributions are either both significant or both negligible. Specific situations in which the gradient term dominates are, however, of considerable interest in applications. The parameters which characterize the anisotropy of collision cascades also determine the deposition of momentum, but the connection is less straightforward than asserted hitherto.

General principles are first illustrated on the specific case of elastic-collision cascades under self-bombardment which contains the essentials. Thereafter several generalizations are made, including atomic binding forces and inelasticity as well as allowance for multicomponent materials. Application areas in mixing and sputtering are outlined.

M. W. Sckerl and P. Sigmund
Physics Department
Odense University
DK-5230 Odense M, Denmark

M. Vicanek
Institut für Theoretische Physik
Technische Universität
D-38023 Braunschweig, Germany

Contents

1	Introduction	5
2	Fundamentals	6
2.1	Particle Density and Flux Density	6
2.2	Freezing Density, Deposited Energy, and Deposited Momentum	7
2.3	Connections	8
2.4	Elastic Scattering	10
2.5	Inelastic Processes	10
3	Transport Equations	11
3.1	Forward and Backward Equations	12
3.2	Planar Geometry	13
3.3	Deposited Energy and Momentum	13
4	Moment Equations	14
4.1	General	14
4.2	Elastic Scattering and Power Cross Section	15
4.3	High-Energy Expansion	16
4.4	Choice of Exponent	19
4.5	Symmetry Considerations	20
4.6	Deposited Energy and Momentum	21
5	Depth Profiles	22
5.1	Approximate Expression for Flux Density	22
5.2	Deposited Momentum	23
5.3	Inverse Relationships	24
5.4	Divergencies	24
5.5	Physical Origin of the Gradient Term	25
6	Generalizations	26
6.1	Non-Selfbombardment	26
6.2	Electronic Stopping: High-Energy Correction	28
6.3	Role of Binding	30
6.4	Electronic Stopping: Low-Energy Correction	32
6.5	More General Cross Sections	33
6.6	Isotope Effect	34
7	Results	36
7.1	Moments	36

7.2	Construction of Profiles	36
7.3	Monte Carlo Simulation	37
7.4	Deposited Momentum and Energy	38
7.5	Flux Density	40
7.6	General Behavior of the Anisotropy Factor	44
7.7	Power-Law Anisotropy	47
8	Discussion	48
8.1	Deposited Momentum and Energy	48
8.2	Particle Flux in Bulk	49
8.3	Collisional Mixing	50
8.4	Particle Flux at Surface	51
8.5	Sputter Yield	52
8.6	Differential Sputter Fluxes	52
8.7	Isotope Effect	53
	Appendix	54
A	Polyatomic Materials	54
A.1	Fundamentals	54
A.2	Transport Equations	56
A.3	Solutions	57
B	Conservation Laws	58
B.1	Energy Conservation	58
B.2	Momentum Conservation	60
B.3	Applications	61
	Acknowledgements	62
	References	62

1 Introduction

Energetic particles like ions, neutrons, and electrons may induce cascades of recoil atoms when interacting with matter. Such atomic collision cascades lead to a variety of observable radiation effects in solid or liquid materials such as defect formation and sputtering, disordering and mixing, and phase transitions. Collision cascades may also influence electronic effects such as ionization and electron or photon emission in both gaseous and condensed matter.

The number of atoms participating in a collision cascade is dependent primarily on the available energy, where key parameters are the binding energy of a recoiling atom to its original site, the cross section for subthreshold (non-recoil) scattering events, and the rate of electronic excitation (LINDHARD ET AL., 1963a; SIGMUND, 1969a, 1972).

Except for effects caused by regular crystal structure, the overall velocity distribution of recoiling atoms is close to isotropic if the number of participating atoms is large, i.e., if the initial energy is high compared to the binding energy. Directional memory is lost rapidly since atoms recoil most frequently at large angles from the initial direction of a colliding particle. Some degree of preferred motion must yet prevail because of conservation of the momentum of the initiating particle (SANDERS, 1968).

The approximation of an isotropic recoil cascade has also been imposed on the *local* velocity distribution of moving atoms in limited regions in space as a consequence of heavy-ion bombardment (THOMPSON, 1968), where its validity is not obvious. A detailed study provided support in the asymptotic limit, i.e., for recoil energies far below the initial beam energy (SIGMUND, 1969b), but only very qualitative information was provided on where the approximation breaks down. Even in the asymptotic limit there can be little doubt that in the outer regions of a collision cascade the motion must be preferentially directed outward.

Several attempts have been made to estimate the dependence of local anisotropy in a collision cascade on the masses of the participating atoms as well as primary and recoil energy. These attempts were based on the recognition that both the overall and the local anisotropy in a cascade must be related to momentum conservation (ROOSENDAAL ET AL., 1980, 1982; SIGMUND, 1981).

Momentum-induced anisotropy in collision cascades came up again in connection with attempts to understand pronounced preferential sputtering effects from isotopic mixtures that were predicted by molecular-dynamics computer simulations (SHAPIRO ET AL., 1985, 1988). While an analysis by two of us did not confirm the assertion that momentum anisotropy was a factor of major importance in this context (SIGMUND & SCKERL, 1993), several problems had been left open in previous studies of momentum anisotropy. There were ambiguities attached to the very

definition of the term ‘deposited momentum’, in particular at the low-energy end of the cascade (URBASSEK & VICANEK, 1992). Moreover, the accurate connection between deposited momentum and particle flux had never been established. One of us had published an approximate relation between particle flux and deposited momentum long ago in a review without documentation (SIGMUND, 1981), and relations have appeared in the literature that are either misleading or wrong (ROOSENDAAL ET AL., 1980, 1982). Moreover, spurious divergencies were found, the origin of which has been discussed only recently (SCKERL ET AL., 1995; GLAZOV, 1995), even though it has been clear for some time that there is no real problem if more terms are taken into account (ROOSENDAAL ET AL., 1982). Altogether, published information on either momentum deposition profiles or angular distributions of particle fluxes is sparse to say the least.

In view of this state of affairs we found it desirable to analyse the whole complex of problems in some detail. We define key parameters from first principles and consider their mutual relationships to some degree of generality. In that respect, this work may be considered as an extension of a previous discussion of scalar quantities (HUANG ET AL., 1985).

The paper has been organized such that the discussion focuses initially on self-bombardment of a single-component material of infinite extension. Extension to more general bombardment conditions is discussed subsequently while results applying to a multicomponent material have been collected in appendix A. Explicit analytic results will be presented for the case where scattering is assumed elastic and governed by a power-law cross section. Arguments will be given which allow generalization to a wider variety of scattering laws, and explicit estimates will be given of the effects of electronic stopping and lattice binding forces. Results of this project were reported at a recent conference (SCKERL ET AL., 1995).

2 Fundamentals

2.1 Particle Density and Flux Density

Consider some source of radiation, typically an ion beam or a source of fast neutrons, which generates energetic particles via collision cascades in a polyatomic medium, the composition of which may be characterized by a set of density profiles $N_j(\mathbf{r})$, where $j = 1, 2, \dots, n$ in an n -atomic medium and $N_j(\mathbf{r})d^3\mathbf{r}$ is the mean number of j -atoms in a volume element $d^3\mathbf{r}$. For high irradiation fluences this profile may depend on time. If so, $N_j(\mathbf{r})$ is meant to denote the profile seen by an individual incident beam particle. As a result of the interaction between one beam particle and the material a cascade of atomic collisions develops which may be characterized by a density $g_j(\mathbf{w}, \mathbf{r}, t)$ of moving particles in phase space such

that $g_j(\mathbf{w}, \mathbf{r}, t)d^3\mathbf{w}d^3\mathbf{r}$ is the mean number of j -atoms moving in volume elements $(\mathbf{r}, d^3\mathbf{r})$ and $(\mathbf{w}, d^3\mathbf{w})$ in real and velocity space, respectively, at time t . The average is taken over a large number of primary impacts with identical initial conditions as far as measurable beam and target parameters are concerned.

For the purpose of the present study the central quantity is the time-integrated flux density,

$$G_j(\mathbf{w}, \mathbf{r}) = w \int_0^\infty dt g_j(\mathbf{w}, \mathbf{r}, t) \quad (1)$$

which is known from transport theory to play the role of a Green function from which several other statistical distributions may be derived (DUDERSTADT & MARTIN, 1979).

It will frequently be necessary to include a specification of the initiating particle in the definition of the density. Then the notation $g_{ij}(\mathbf{v}; \mathbf{w}, \mathbf{r}, t)$ implies that the collision cascade has been initiated by an i -particle impinging with a velocity \mathbf{v} in $\mathbf{r} = 0$ at $t = 0$. Here an i -particle may be either an external particle ($i = 0$) or an energetic recoil atom of the material ($i = 1, \dots, n$). Similar extensions apply to the flux density and other statistical distributions to be introduced in the following.

The essential arguments to be presented in the following apply equally well to self-bombardment of a monoatomic medium as to arbitrary bombardment of an arbitrary medium, but discussing the former allows for a simpler notation and, hence, a more transparent presentation. Therefore the bulk of the paper emphasizes self-bombardment of a monoatomic medium. More general results have been collected in section 6.1 on pp. 26 for non-selfbombardment and in appendix A for polyatomic media. Reference to these sections will be made where appropriate. This eliminates the need for atom labels here. We may then operate with a particle density $g(\mathbf{w}, \mathbf{r}, t)$ and a flux density $G(\mathbf{w}, \mathbf{r})$.

2.2 Freezing Density, Deposited Energy, and Deposited Momentum

Consider now some energy U below which all motion of beam and recoil particles is assumed to be frozen in. We introduce the freezing density $F(\mathbf{w}, \mathbf{r}, U)$ which reflects the distribution in real and velocity space of a cascade after all participating atoms have slowed down below U . Thus, $F(\mathbf{w}, \mathbf{r}, U)d^3\mathbf{w}d^3\mathbf{r}$ is the mean number of atoms per incident particle emerging from collisions in a volume element $(\mathbf{r}, d^3\mathbf{r})$ at velocities in an interval $(\mathbf{w}, d^3\mathbf{w})$ with

$$W \equiv Mw^2/2 < U, \quad (2)$$

when cascade processes are recorded only for particles with energies above U . Here, M denotes the mass of the particles involved.

Except for the name the freezing density was introduced into this field by SANDERS (1968). It makes possible a precise definition of the useful concepts of deposited energy and momentum,

$$F_D(\mathbf{r}, U) = \int_{W < U} d^3\mathbf{w} W F(\mathbf{w}, \mathbf{r}, U)$$

$$F_P(\mathbf{r}, U) = \int_{W < U} d^3\mathbf{w} M \mathbf{w} F(\mathbf{w}, \mathbf{r}, U).$$
(3)

For an elastic-collision cascade¹, the integral over all space of these distributions must equal the initial energy and momentum of the beam particle, respectively, irrespective of the choice of U .

In addition to densities of deposited energy and momentum one may also consider the associated current densities or fluxes. Conservation laws satisfied by these quantities have the form of continuity equations which have been collected in appendix B.

2.3 Connections

The leading term in the standard expression for the particle flux in the limit of high ion energy is approximately proportional to the density of deposited energy (SIGMUND, 1969b). It is also known that corrections to this term depend on the deposited momentum (SANDERS, 1968; SIGMUND, 1981). Before discussing those important connections we derive the inverse relationships which, unlike the former, are exact since the flux density is a Green function.

In the following we shall assume a random distribution of scattering centers in the material. The connection between the freezing density and the particle density is found most conveniently by a physical argument. Indeed, write

$$F(\mathbf{w}, \mathbf{r}, U) = N(\mathbf{r}) \int_{W' > U} d^3\mathbf{w}' \int_0^\infty dt w' g(\mathbf{w}', \mathbf{r}, t) \int d\sigma(\mathbf{w}'; \mathbf{v}', \mathbf{v}'')$$

$$\times \left(\delta(\mathbf{v}' - \mathbf{w}) + \delta(\mathbf{v}'' - \mathbf{w}) \right). \quad (W < U) \quad (4)$$

Here, $d\sigma(\mathbf{v}; \mathbf{v}', \mathbf{v}'')$ is the differential cross section for scattering of an atom with a velocity \mathbf{v} hitting an atom at rest, \mathbf{v}' and \mathbf{v}'' denoting the respective velocities after collision, and $\delta(\dots)$ is the Dirac function. By definition, $d^3\mathbf{w}' g(\mathbf{w}', \mathbf{r}, t)$ represents the mean number of particles per volume moving with velocity $(\mathbf{w}', d^3\mathbf{w}')$ at time

¹By definition, the sum of the kinetic energies of all particles in motion is constant in an elastic-collision cascade. The effect of two major sources of inelasticity, electronic stopping of primary and target recoil atoms, and binding of target atoms, will be studied in sections 6.2 - 6.4.

t , and $N(\mathbf{r})w'dtd\sigma(\mathbf{w}';\mathbf{v}',\mathbf{v}'')$ is the probability for a collision with the outcome $(\mathbf{v}',d^3\mathbf{v}')$, $(\mathbf{v}'',d^3\mathbf{v}'')$. The contents of the parentheses represent the probability density for either the colliding or the recoiling atom to have a final velocity around \mathbf{w} .

We identify the flux density (1) in eq. (4) and insert into eqs. (3) with the result

$$F_D(\mathbf{r},U) = N(\mathbf{r}) \int_{W>U} d^3\mathbf{w} G(\mathbf{w},\mathbf{r}) \left(\int_{E'<U} E' d\sigma + \int_{E''<U} E'' d\sigma \right) \quad (5)$$

$$\mathbf{F}_P(\mathbf{r},U) = N(\mathbf{r}) \int_{W>U} d^3\mathbf{w} G(\mathbf{w},\mathbf{r}) \left(\int_{E'<U} M\mathbf{v}' d\sigma + \int_{E''<U} M\mathbf{v}'' d\sigma \right) \quad (6)$$

where $E' = Mv'^2/2$ and $E'' = Mv''^2/2$ represent the energies of the scattered atom and the recoil, respectively.

Differential cross sections most often exhibit azimuthal symmetry around the direction of the colliding atom. If so, the first integral in the parentheses of eq. (6) reduces to

$$\int_{E'<U} M\mathbf{v}' d\sigma(\mathbf{w};\mathbf{v}',\mathbf{v}'') = \frac{\mathbf{w}}{w} \int_{E'<U} Mv' \cos\phi' d\sigma$$

where ϕ' denotes the scattering angle in the laboratory system. A corresponding expression holds for the second integral.

It is common to replace velocities by energy and angular variables

$$G(\mathbf{w},\mathbf{r})d^3\mathbf{w} \equiv G(W,\mathbf{\Omega},\mathbf{r})dWd^2\mathbf{\Omega} \quad (7)$$

where $\mathbf{\Omega} = \mathbf{w}/w$ is a unit vector in the direction of the velocity \mathbf{w} . Then eqs. (5) and (6) reduce to

$$F_D = N \int_{W>U} dW G(W) \left(\int_{E'<U} E' d\sigma + \int_{E''<U} E'' d\sigma \right) \quad (8)$$

$$\mathbf{F}_P = N \int_{W>U} dW \mathbf{H}(W) \left(\int_{E'<U} Mv' \cos\phi' d\sigma + \int_{E''<U} Mv'' \cos\phi'' d\sigma \right)$$

where

$$\begin{aligned} G(W) &= \int d^2\mathbf{\Omega} G(W,\mathbf{\Omega}) \\ \mathbf{H}(W) &= \int d^2\mathbf{\Omega} \mathbf{\Omega} G(W,\mathbf{\Omega}). \end{aligned} \quad (9)$$

The spatial variable \mathbf{r} has been suppressed for clarity and ϕ'' denotes the recoil angle in the laboratory system.

Eqs. (8) represent rigorous expressions for the densities of deposited energy and momentum in terms of the flux density $G(W, \Omega)$. An approximate expression for the inverse relationship – which is of much greater practical importance – will be found in section 5.1 (p. 22).

2.4 Elastic Scattering

Now assume elastic collisions. For equal-mass colliding particles we may write

$$\begin{aligned} E' &= E - T; & E'' &= T \\ Mv' \cos \phi' &= \frac{2}{w}(E - T); & Mv'' \cos \phi'' &= \frac{2}{w} T \end{aligned} \quad (10)$$

where T is the energy transfer in conventional notation. Then eqs. (8) reduce to

$$F_D = N \int_{W>U} dW G(W) (S'(W, U) + S''(W, U)) \quad (11)$$

$$F_P = N \int_{W>U} dW \frac{2}{w} \mathbf{H}(W) (S'(W, U) + S''(W, U)) \quad (12)$$

where

$$\begin{aligned} S'(W, U) &= \int_{W-T < U} (W - T) d\sigma(W, T) \\ S''(W, U) &= \int_{T < U} T d\sigma(W, T) \end{aligned} \quad (13)$$

and $d\sigma(W, T)$ is the differential cross section for energy transfer (T, dT) from an atom with kinetic energy W to an atom at rest. With this, the same transport cross sections occur in both deposited energy and deposited momentum.

2.5 Inelastic Processes

Scattering processes between atoms are more or less inelastic because energy is spent in electronic excitation and ionization. This is known to affect the energy balance (LINDHARD ET AL., 1963a); a similar effect on momentum balance must be expected. We need to distinguish between the influence of inelastic losses on particle flux, deposited energy and momentum on the one hand, and the influence of such losses on the relations connecting them. Here we are concerned only about the latter aspect. The effect of electronic stopping on the quantities themselves is going to be considered in sections 6.2 and 6.4.

We shall employ a scheme introduced by LINDHARD ET AL. (1963a,b) in which electronic interactions are treated as occurring between two separate systems, electrons and nuclei. This scheme does not properly account for inner-shell processes and other forms of strong coupling but is well suited in cases where electronic processes are expected to cause minor perturbations. Temporarily we introduce separate flux densities $G^{(n)}$ and $G^{(e)}$ for atoms and electrons as well as separate expressions $F_D^{(n)}$, $F_D^{(e)}$ and $F_P^{(n)}$, $F_P^{(e)}$ for energy and momentum deposited in atomic and electronic motion, respectively. Going through the above arguments one arrives at an expression for $F_D^{(n)}$ containing two terms, one identical with eq. (11), $G(W)$ being replaced by $G^{(n)}(W)$. The second contribution is a coupling term of the form

$$\Delta F_D^{(n)} = N \int dW G^{(e)}(W) \int_{T < U} T d\sigma_{\text{en}}(W, T)$$

where $d\sigma_{\text{en}}(W, T)$ is the differential cross section for scattering of an electron of energy W on an atom. Similarly the momentum term receives an addition of the form

$$\Delta F_P^{(n)} = N \int dW \mathbf{H}^{(e)}(W) \int_{T < U} \sqrt{2MT} \cos \phi'' d\sigma_{\text{en}}(W, T).$$

In the conventional picture (LINDHARD ET AL., 1963a,b) any transfer of energy from electronic to nuclear motion is ignored because of the large difference in mass between nuclei and electrons. To the extent that this picture is valid it should also apply to deposited momentum because the total amount of momentum contained in electronic motion is small. On the other hand, numerous processes have been identified, in particular in insulators, which efficiently transfer energy from electronic to nuclear motion (JOHNSON & SCHOU, 1993; REIMANN, 1993). Whenever one of those processes is active the above coupling term between energy deposited in atomic motion and the electron flux needs to be taken into account.

Equations expressing the energy and momentum deposited in *electronic* motion may be established by interchanging labels ‘n’ and ‘e’. Here the coupling term will in general not be negligible.

3 Transport Equations

In the following we shall assume the density of moving atoms to be low enough that the neglect of collisions between moving atoms be justified. Collisions are formally taken as binary, but this does not preclude taking into account distant simultaneous interactions with several particles as long as they may be described within first-order perturbation theory.

On the basis of the above assumptions one arrives at linear transport equations which are wellknown (SIGMUND, 1972, 1991). These equations may be written in

forward or backward form. For a homogeneous stopping medium the two forms are equivalent. They differ in the roles played by the instantaneous velocity variable \mathbf{w} and the initial velocity \mathbf{v} .

3.1 Forward and Backward Equations

The particle density $g(\mathbf{w}, \mathbf{r}, t)$ is a convenient starting point. The forward Boltzmann equation reads

$$\frac{\partial g(\mathbf{w})}{\partial t} + \mathbf{w} \cdot \nabla g(\mathbf{w}) = N \int d^3 \mathbf{w}' \int d^3 \mathbf{w}'' \left\{ w' g(\mathbf{w}') K(\mathbf{w}'; \mathbf{w}, \mathbf{w}'') \right. \\ \left. + w' g(\mathbf{w}') K(\mathbf{w}'; \mathbf{w}'', \mathbf{w}) - w g(\mathbf{w}) K(\mathbf{w}; \mathbf{w}', \mathbf{w}'') \right\}, \quad (14)$$

where $K(\mathbf{w}; \mathbf{w}', \mathbf{w}'') d^3 \mathbf{w}' d^3 \mathbf{w}'' \equiv d\sigma(\mathbf{w}; \mathbf{w}', \mathbf{w}'')$. Eq. (14) follows readily from a comparison of $g(\mathbf{w}, \mathbf{r}, t + \delta t)$ with $g(\mathbf{w}, \mathbf{r}, t)$ since $N w d\sigma$ is the collision rate per unit time. The time and space variables have been suppressed for clarity. The particle density N in the medium will henceforth be taken constant.

The corresponding equation for the particle flux is found by integration over time with the initial condition $g(\mathbf{w}, \mathbf{r}, 0) = \delta(\mathbf{r})\delta(\mathbf{w} - \mathbf{v})$,

$$N \int d^3 \mathbf{w}' \int d^3 \mathbf{w}'' \left\{ G(\mathbf{w}) K(\mathbf{w}; \mathbf{w}', \mathbf{w}'') - G(\mathbf{w}') K(\mathbf{w}'; \mathbf{w}, \mathbf{w}'') \right. \\ \left. - G(\mathbf{w}') K(\mathbf{w}'; \mathbf{w}'', \mathbf{w}) \right\} + \boldsymbol{\Omega} \cdot \nabla G(\mathbf{w}) = \delta(\mathbf{w} - \mathbf{v})\delta(\mathbf{r}). \quad (15)$$

The backward equation for the particle density reads

$$\frac{\partial g(\mathbf{v})}{\partial t} + \mathbf{v} \cdot \nabla g(\mathbf{v}) = N v \int d\sigma(\mathbf{v}; \mathbf{v}', \mathbf{v}'') \left\{ g(\mathbf{v}') + g(\mathbf{v}'') - g(\mathbf{v}) \right\},$$

where the variables \mathbf{w}, \mathbf{r} , and t all have been suppressed. Several ways to derive these equations have been outlined in the literature (LINDHARD ET AL., 1963a, 1971; SIGMUND, 1969b, 1991) but will not be reproduced here. Integration over time with the above initial condition yields the flux equation

$$N \int d\sigma(\mathbf{v}; \mathbf{v}', \mathbf{v}'') \left\{ G(\mathbf{v}) - G(\mathbf{v}') - G(\mathbf{v}'') \right\} + \mathbf{e} \cdot \nabla G(\mathbf{v}) = \delta(\mathbf{v} - \mathbf{w})\delta(\mathbf{r}) \quad (16)$$

where $\mathbf{e} = \mathbf{v}/v$ is a unit vector in the direction of the initial velocity \mathbf{v} .

The linearity of eqs. (15) and (16) and the occurrence of the Dirac functions on the right-hand side make it formally clear that the particle flux is a Green function. The velocity variable \mathbf{w} is an active variable in the forward equation but mute in the backward equation. Therefore the backward equation allows integration over \mathbf{w}

with an arbitrary weight function and, hence, derivation of a transport equation for quantities that can be derived from the particle flux. Consequently such equations are identical with eq. (16) except for the inhomogeneity on the right-hand side. This holds in particular for the transport equations obeyed by deposited energy and momentum.

3.2 Planar Geometry

The assumption of an infinite random scattering medium implies isotropy. Therefore the particle flux can depend only on two rather than three independent directional variables. We may fix one directional variable according to convenience without loss of generality. Although the ‘natural’ directional variable is the beam direction as expressed by \mathbf{v} , for many purposes in ion beam physics it is more convenient to keep the direction of the spatial variable \mathbf{r} fixed. For a semi-infinite target with a plane surface the x -axis is chosen along the inward surface normal. For an infinite medium the choice is arbitrary. In either case the particle flux and all derived quantities will be integrated over the lateral coordinates (y, z) . Then eqs. (15) and (16) reduce to

$$N \int d^3 \mathbf{w}' \int d^3 \mathbf{w}'' \left\{ G(\mathbf{w}) K(\mathbf{w}; \mathbf{w}', \mathbf{w}'') - G(\mathbf{w}') K(\mathbf{w}'; \mathbf{w}, \mathbf{w}'') - G(\mathbf{w}') K(\mathbf{w}'; \mathbf{w}'', \mathbf{w}) \right\} + \cos \theta \frac{\partial G(\mathbf{w})}{\partial x} = \delta(\mathbf{w} - \mathbf{v}) \delta(x) \quad (17)$$

and

$$N \int d\sigma(\mathbf{v}; \mathbf{v}', \mathbf{v}'') \left\{ G(\mathbf{v}) - G(\mathbf{v}') - G(\mathbf{v}'') \right\} + \cos \Theta \frac{\partial G(\mathbf{v})}{\partial x} = \delta(\mathbf{v} - \mathbf{w}) \delta(x) \quad (18)$$

where θ and Θ are the angles between the instantaneous velocity \mathbf{w} and the initial velocity \mathbf{v} and the x axis, respectively. These two relations form the starting point for solutions of the transport problem.

3.3 Deposited Energy and Momentum

Deposited energy $F_D(\mathbf{v}, \mathbf{r}, U)$ and momentum $\mathbf{F}_P(\mathbf{v}, \mathbf{r}, U)$ obey backward transport equations. These equations are identical with the one satisfied by the flux density eq. (18) except for the inhomogeneity on the right-hand side. For planar geometry and $E > U$ we find

$$N \int d\sigma(\mathbf{v}; \mathbf{v}', \mathbf{v}'') \left\{ F_D(\mathbf{v}) - F_D(\mathbf{v}') - F_D(\mathbf{v}'') \right\} + \cos \Theta \frac{\partial}{\partial x} F_D(\mathbf{v}) = 0 \quad (19)$$

$$N \int d\sigma(\mathbf{v}; \mathbf{v}', \mathbf{v}'') \left\{ \mathbf{F}_P(\mathbf{v}) - \mathbf{F}_P(\mathbf{v}') - \mathbf{F}_P(\mathbf{v}'') \right\} + \cos \Theta \frac{\partial}{\partial x} \mathbf{F}_P(\mathbf{v}) = 0 \quad (20)$$

where, for convenience of notation, the inhomogeneities on the right-hand side have been replaced by normalization conditions

$$\int_{-\infty}^{\infty} dx F_D(\mathbf{v}, x, U) = E \quad \text{for } E < U \quad (21)$$

$$\int_{-\infty}^{\infty} dx \mathbf{F}_P(\mathbf{v}, x, U) = M\mathbf{v} \quad \text{for } E < U. \quad (22)$$

4 Moment Equations

4.1 General

For an infinite medium a convenient way to solve transport equations goes over spatial moments. We follow the procedure applied previously (SANDERS, 1968; SIGMUND, 1969b; WINTERBON ET AL., 1970) and take the backward equation (18) as a starting point. Expand the flux in terms of the angular variables,

$$G(E, \mathbf{e}; W, \boldsymbol{\Omega}, x) = \sum_{\ell, \mu} \sum_{\ell', \mu'} \sqrt{4\pi(2\ell+1)} \sqrt{4\pi(2\ell'+1)} \\ \times G_{\ell, \mu; \ell', \mu'}(E; W, x) Y_{\ell\mu}(\mathbf{e}) Y_{\ell'\mu'}^*(\boldsymbol{\Omega})$$

where energy and directional variables have been introduced just as in eq. (7) on page 9, and $Y_{\ell\mu}(\mathbf{e})$ are spherical harmonics in one of several standard notations. The numerical factors have been chosen such that conventional notation is recovered for $\mu = 0$. Spatial moments are introduced according to

$$G_{\ell, \mu; \ell', \mu'}^{(n)}(E; W) = \int_{-\infty}^{\infty} dx x^n G_{\ell, \mu; \ell', \mu'}(E; W, x).$$

With this the backward equation reduces to the following multi-dimensional set of equations for moments,

$$(2\ell+1)N \int d\sigma(E; E', E'') \left\{ G_{\ell, \mu; \ell', \mu'}^{(n)}(E; W) - P_{\ell}(\cos \phi') G_{\ell, \mu; \ell', \mu'}^{(n)}(E'; W) \right. \\ \left. - P_{\ell}(\cos \phi'') G_{\ell, \mu; \ell', \mu'}^{(n)}(E''; W) \right\} = \delta_{n0} \delta_{\ell\ell'} \delta_{\mu\mu'} \frac{1}{4\pi} \delta(E - W) \\ + n \left(\sqrt{\ell^2 - \mu^2} G_{\ell-1, \mu; \ell', \mu'}^{(n-1)}(E; W) + \sqrt{(\ell+1)^2 - \mu^2} G_{\ell+1, \mu; \ell', \mu'}^{(n-1)}(E; W) \right) \quad (23)$$

where the P_{ℓ} are Legendre polynomials. This system of equations can be solved recurrently starting from $n = 0$.

4.2 Elastic Scattering and Power Cross Section

The case of power-law elastic scattering (LINDHARD ET AL., 1963a, 1968) is a useful reference since it allows finding solutions with a considerable amount of rigor. The cross section is written in the form

$$d\sigma_{ij}(E, T) = C_{ij}E^{-m}T^{-1-m}dT; \quad 0 \leq T \leq \gamma_{ij}E, \tag{24}$$

where $\gamma_{ij} = 4M_iM_j/(M_i + M_j)^2$ and

$$C_{ij} = \frac{\pi}{2}\lambda_m a_{ij}^2 \left(\frac{M_i}{M_j}\right)^m \left(\frac{2Z_1Z_2e^2}{a_{ij}}\right)^{2m}. \tag{25}$$

Here the Z_i and M_i are atomic numbers and masses, respectively, and a_{ij} screening radii for interaction between i and j atoms. The quantity m is an exponent in the interval $0 \lesssim m \leq 1$ and λ_m a dimensionless quantity depending on m and determined by the screening function. It has been shown (LINDHARD ET AL., 1968) that this cross section approximates the scattering law for a power-law interaction potential $\propto R^{-1/m}$, R being the internuclear distance between two interacting atoms. It is also known that screened-Coulomb-type interatomic potentials behave power-like over limited ranges of the internuclear distance. An alternative version of eq. (25) applying to other repulsive potentials was proposed by ANDERSEN & SIGMUND (1974).

The common strategy of solving equations like eq. (23) (ROBINSON, 1965; SIGMUND, 1969c, 1972) is to switch to logarithmic variables $u = \log(E/W)$ and to take the Laplace transform of the moment equation (23). For the monoatomic case where $\gamma_{ij} = 1$ this leads to

$$(2\ell + 1)NCW^{-2m}\overline{G}_{\ell,\mu;\ell',\mu'}^{(n)}(s)I_\ell(s) = \delta_{n0}\delta_{\ell\ell'}\delta_{\mu\mu'}\frac{1}{4\pi W} + n \left(\sqrt{\ell^2 - \mu^2}\overline{G}_{\ell-1,\mu;\ell',\mu'}^{(n-1)}(s-2m) + \sqrt{(\ell+1)^2 - \mu^2}\overline{G}_{\ell+1,\mu;\ell',\mu'}^{(n-1)}(s-2m) \right) \tag{26}$$

with $\overline{G}(s) = \int_0^\infty du \exp(-su)G(u)$ denoting the Laplace transform and

$$I_\ell(s) = \int_0^1 dt t^{-1-m} \left\{ 1 - P_\ell(\cos \phi')(1-t)^s - P_\ell(\cos \phi'')t^s \right\}. \tag{27}$$

For arbitrary masses of collision partners we have

$$\cos \phi' = (1-t)^{1/2} + \alpha_{ij}t(1-t)^{-1/2}; \quad \cos \phi'' = (t/\gamma_{ij})^{1/2} \tag{28}$$

with $\alpha_{ij} = (M_i - M_j)/2M_i$. Eq. (26) represents a system of algebraic equations which can be solved rigorously up to any order n .

4.3 High-Energy Expansion

The solutions in energy space of integral equations of the above type may be written in the form of asymptotic series (SIGMUND, 1969c, 1972),

$$\sum_{\alpha} A_{\alpha}(E/W)^{\alpha}$$

where the α form a monotonically decreasing sequence of real but in general not integer numbers. In Laplace space this reads

$$\sum_{\alpha} A_{\alpha}/(s - \alpha).$$

Therefore, individual terms making up the asymptotic series of any moment may be found by location of poles and determination of residues in the Laplace transform of that moment. For $E \gg W$ the leading terms originate from the poles at the highest values of s .

For $n = 0$ the poles of $\overline{G}_{\ell,\mu;\ell,\mu}(s)$ are identical with the zeros of $I_{\ell}(s)$. For equal masses the function $I_0(s)$ has zeros at $s = 1$ and one each in the intervals $-\nu < s < -(\nu - 1)$ for $\nu = 1, 2, \dots$. Eq. (27) shows that $I_1(s) \equiv I_0(s + 1/2)$ for equal masses and, hence, has its leading zero at $s = 1/2$. All $I_{\ell}(s)$ for $\ell \geq 2$ have zeros only at negative values of s .

In the following only terms differing by at most one power of E/W from the leading term will be taken into account in any moment $G^{(n)}$. This implies that for $n = 0$ only the terms $\propto (E/W)$ for $\ell = 0$ and $\propto (E/W)^{1/2}$ for $\ell = 1$ will be taken as significant. From eq. (26) follows that for $n = 1$ the poles of $\overline{G}^{(1)}(s)$ fall into two groups. One group originates from the pertinent poles in $\overline{G}^{(0)}(s - 2m)$, i.e., poles in $s = 1 + 2m$ and $1/2 + 2m$. The other group originates in the zeros of $I_{\ell}(s)$, primarily $s = 1$ and $1/2$. Similar considerations apply to higher moments. As a result we get the list of moments indicated in table I which, for $0 < m < 1$, either contribute to the leading term for a given n or differ from it by at most a factor of E/W .

Table I shows that all moments may be classified into families. A family originates either in a term $\propto E/W$ or $\propto \sqrt{E/W}$ in any given order n , and for every subsequent generation a factor $(E/W)^{2m}$ is added. The dominating family originates in $(n, \ell) = (0, 0)$. The subsequent two families originate in $(n, \ell) = (0, 1)$ and $(1, 0)$, respectively. The former is in the lead for $m > 1/4$ while the latter dominates for $m < 1/4$. We recall that the prime selection criterion requires to neglect all terms which, at any given order of moment n , differ by more than one power of E/W or E/U from the leading term, i.e., the term originating in $(n, \ell) = (0, 0)$. Within that criterion, the term originating in $(n, \ell) = (0, 1)$ is always significant while the term originating in $(n, \ell) = (1, 0)$ is significant only for $m \leq 1/2$.

Table I. Leading terms in asymptotic expansion of moments over the particle flux; listed are exponents α of $(E/W)^\alpha$. Only moments for $n \leq 3$ listed.

l	0	1	2	3	4
0	1	1/2			
1	1/2 + 2m 1	1 + 2m 1/2	1/2 + 2m		
2	1 + 4m 1/2 + 2m 1	1/2 + 4m 1 + 2m 1/2	1 + 4m 1/2 + 2m	1/2 + 4m	
3	1/2 + 6m 1 + 4m 1/2 + 2m 1	1 + 6m 1/2 + 4m 1 + 2m 1/2	1/2 + 6m 1 + 4m 1/2 + 2m	1 + 6m 1/2 + 4m	1/2 + 6m

Another two families derive from $(n, \ell) = (1, 1)$ and $(2, 0)$. Again the former dominates for $m > 1/4$ and the latter for $m < 1/4$ but both are significant only for $m < 1/4$. Of the two families originating in $(n, \ell) = (2, 1)$ and $(3, 0)$ the former is significant for $m < 1/8$, the latter for $m < 1/6$, etc. It is seen that the number of significant families increases when m approaches zero.

We shall argue in section 4.4 that only the leading three families need to be considered. Then we obtain

$$G_{\ell, \mu; \ell', \mu'}^{(n)} = \frac{\delta_{\mu\mu'} \Gamma_m}{4\pi NS(W)} \left[\delta_{\ell'0} \delta_{\mu0} \frac{E}{W} \mathcal{A}_\ell^{(n)} \left(\frac{E^{2m}}{NC} \right)^n + \frac{1}{3} \delta_{\ell'1} \sqrt{\frac{E}{W}} \mathcal{B}_{\ell, \mu}^{(n)} \left(\frac{E^{2m}}{NC} \right)^n + \frac{1}{3} \delta_{\ell'1} \delta_{\mu0} \frac{1}{I_1(1-2m)} \frac{E}{W} \frac{W^{2m}}{NC} \mathcal{C}_\ell^{(n)} \left(\frac{E^{2m}}{NC} \right)^{n-1} \right] \quad (29)$$

Table II. Same as table I but ordered into \mathcal{A} -, \mathcal{B} -, and \mathcal{C} -families.

Family	l n	0	1	2	3	4
\mathcal{A}	0	1				
	1		$1 + 2m$			
	2	$1 + 4m$		$1 + 4m$		
	3		$1 + 6m$		$1 + 6m$	
\mathcal{B}	0		$1/2$			
	1	$1/2 + 2m$		$1/2 + 2m$		
	2		$1/2 + 4m$		$1/2 + 4m$	
	3	$1/2 + 6m$		$1/2 + 6m$		$1/2 + 6m$
\mathcal{C}	0					
	1	1				
	2		$1 + 2m$			
	3	$1 + 4m$		$1 + 4m$		

where

$$\Gamma_m = \frac{m}{\psi(1) - \psi(1 - m)}; \quad \psi(\xi) = \frac{d \log \Gamma(\xi)}{d\xi}. \tag{30}$$

Moreover,

$$S(W) = \frac{1}{1 - m} CW^{1-2m} \tag{31}$$

is the stopping cross section. The numerical coefficients are determined by the recurrence relations

$$\begin{aligned} \mathcal{A}_\ell^{(n)} &= \frac{n}{2\ell + 1} \frac{\ell \mathcal{A}_{\ell-1}^{(n-1)} + (\ell + 1) \mathcal{A}_{\ell+1}^{(n-1)}}{I_\ell(1 + 2mn)} \\ \mathcal{B}_{\ell,\mu}^{(n)} &= \frac{n}{2\ell + 1} \frac{\sqrt{\ell^2 - \mu^2} \mathcal{B}_{\ell-1,\mu}^{(n-1)} + \sqrt{(\ell + 1)^2 - \mu^2} \mathcal{B}_{\ell+1,\mu}^{(n-1)}}{I_\ell(1/2 + 2mn)} \\ \mathcal{C}_\ell^{(n)} &= \frac{n}{2\ell + 1} \frac{\ell \mathcal{C}_{\ell-1}^{(n-1)} + (\ell + 1) \mathcal{C}_{\ell+1}^{(n-1)}}{I_\ell(1 + 2m(n - 1))} \end{aligned} \tag{32}$$

and the initial values

$$\mathcal{A}_0^{(0)} = \mathcal{B}_{1\mu}^{(0)} = \mathcal{C}_0^{(1)} = 1.$$

The recurrence scheme for the three families is illustrated in table II.

4.4 Choice of Exponent

Realistic atomic interaction potentials are screened-Coulomb like, i.e., close to R^{-1} at small internuclear distances and steeper at greater interaction distances. This feature translates into power-like elastic scattering cross sections but with energy-dependent exponents m such that m decreases with decreasing projectile energy. A reasonably reliable procedure for fixing m may be based on the stopping cross section, calculated accurately for a given interaction potential and matched in value and slope by a power law as a function of energy.

Collision cascades are typically initiated by a high-energy particle but the majority of atoms set in motion has quite low initial energies. The question then arises of the choice of exponent m to properly characterize the development of a cascade. The answer is that one exponent is insufficient in general but that the m -values appropriate to the initial velocity \mathbf{v} and the instantaneous velocity \mathbf{w} jointly provide an adequate description (SIGMUND, 1969b). Since the point is central we briefly go through the argument.

Choose the moment $G_{0,0;1,0}^{(1)}$ as a representative example. According to table I the leading terms in the asymptotic expansion go $\propto (E/W)^{1/2+2m}$ and $\propto E/W$, respectively. Eq. (23) on page 14 reads

$$N \int d\sigma(E; E', E'') \left\{ G_{0,0;1,0}^{(1)}(E; W) - G_{0,0;1,0}^{(1)}(E'; W) - G_{0,0;1,0}^{(1)}(E''; W) \right\} = G_{1,0;1,0}^{(0)}(E; W) \quad (33)$$

where $G_{1,0;1,0}^{(0)}(E; W)$ is asymptotically $\propto (E/W)^{1/2}$ according to table I. Now insert $G_{0,0;1,0}^{(1)} \propto (E/W)^{1/2+2m}$ and the power cross section for $d\sigma$. This results in

$$G_{0,0;1,0}^{(1)}(E; W) = G_{1,0;1,0}^{(0)}(E; W) \frac{E^{2m}/NC}{I_0(1/2 + 2m)}$$

which is valid asymptotically. Note that $I_0(1/2 + 2m)$ is a finite nonvanishing number except for $m = 1/4$. On the other hand, when $G_{0,0;1,0}^{(1)} \propto E/W$ is inserted into eq. (33) the left-hand side vanishes everywhere except near the integration boundaries where the asymptotic expressions must be inaccurate. Here subsequent terms in the asymptotic expansion of $G_{0,0;1,0}^{(1)}(E; W)$ need to be taken into account. Since it is the low-energy behavior of $G_{0,0;1,0}^{(1)}(E; W)$ which determines the slope of this linear function it must be the low-energy value of m , i.e., the value appropriate to the energy range around W , that is relevant in this evaluation.

The above argument may be applied to all terms listed in table I. As a result we conclude that exponents $2m$ reflect the length scale E^{2m}/NC of the collision cascade taken at its initial energy while powers E/W and $\sqrt{E/W}$ are governed by

the low-energy behavior. This may be rephrased differently: After classification of all contributing terms into families as noted above, the origin of each family is governed by the low-energy behavior. The recurrence scheme for higher-order moments, as expressed by eqs. (32) as well as the factors $(E^{2m}/NC)^n$ in eq. (29), on the other hand, concerns the overall dimensions of the cascade. Therefore these factors are determined by the high-energy scattering law.

The asymptotic expansion of the particle flux is meaningful only so long as $E \gg W$. This implies that in order to arrive at meaningful results we shall have to assume E to be large enough that for common interaction potentials the exponent m valid at E exceeds the low-energy value $m \sim 1/6$. This implies that the families originating in $(n, \ell) = (1, 1)$ and $(2, 0)$, which are significant only for $m < 1/8$ and $m < 1/6$, may be ignored. The same is true for all families originating in higher moments. Then any significant moment over the particle flux must belong to one of the three families entering into eq. (29) and indicated in table II.

4.5 Symmetry Considerations

An important point of consideration is the dependence of moments on the directional variable Ω which is expressed by the labels ℓ', μ' of the significant terms. For moments of zero'th order, $n = 0$, only terms with $\ell' = \ell$ and $\mu' = \mu$ contribute according to eq. (26) on page 15. This implies that the leading \mathcal{A} family of moments, originating in $\ell = \mu = 0$ and hence $\ell' = \mu' = 0$, does not introduce any dependence on Ω into the underlying distribution. Therefore that part of the flux density must be isotropic. It is the flux density utilized in sputter theory (SIGMUND, 1969b, 1981).

The \mathcal{B} family, also originating in the zero'th order, stems from $\ell' = \ell = 1$ and, consequently, $\mu = \mu' = 1, 0, -1$. This dependence propagates into higher orders. The angular dependence is centered around the incoming direction via $e \cdot \Omega = (4\pi/3) \sum_{\mu} Y_{1\mu}(e) Y_{1\mu}^*(\Omega)$.

The third significant family, \mathcal{C} , originates in $n = 1$ and $\ell = \mu = 0$. In Laplace space this term becomes proportional to the zero-order moment $\ell = \ell' = 1$, $\mu = \mu' = 0$ and therefore carries with it a factor $\cos\theta = \Omega \cdot e_x$ that propagates into higher orders in n . Here, e_x denotes a unit vector along the x -axis.

It is evident that our classification of moments into families according to their dependences on ion energy at the same time implies a separation of the underlying flux distribution into three contributions, each of which has its characteristic dependence on Ω .

4.6 Deposited Energy and Momentum

Moment equations for deposited energy and momentum are established in close analogy to those for the particle flux. After expansion in terms of spherical harmonics

$$F_D(\mathbf{v}; x, U) \equiv \sum_{\ell, \mu} \sqrt{4\pi(2\ell + 1)} F_{D, \ell, \mu}(E; x, U) Y_{\ell\mu}(\mathbf{e})$$

and taking spatial moments $F_{D, \ell, \mu}^{(n)}(E; U) = \int_{-\infty}^{\infty} dx x^n F_{D, \ell, \mu}(E; x, U)$ one finds the following set of moment equations,

$$\begin{aligned} (2\ell + 1)N \int d\sigma(E; E', E'') & \left\{ F_{D, \ell, \mu}^{(n)}(E; U) \right. \\ & \left. - P_\ell(\cos \phi') F_{D, \ell, \mu}^{(n)}(E'; U) - P_\ell(\cos \phi'') F_{D, \ell, \mu}^{(n)}(E''; U) \right\} \\ & = n \left(\sqrt{\ell^2 - \mu^2} F_{D, \ell-1, \mu}^{(n-1)}(E; U) + \sqrt{(\ell + 1)^2 - \mu^2} F_{D, \ell+1, \mu}^{(n-1)}(E; U) \right). \end{aligned} \quad (34)$$

These equations may be solved recurrently starting from $n = 0$ where the normalization condition (21) on page 14 reduces to

$$F_{D, \ell, \mu}^{(0)}(E; U) = \delta_{\ell 0} \delta_{\mu 0} E \quad \text{for } E < U. \quad (35)$$

Definitions and moment equations for $\mathbf{F}_{P, \ell, \mu}^{(n)}$ are analogous with those for F_D but the normalization condition (22) leads to

$$\mathbf{F}_{P, \ell, \mu}^{(0)}(E; U) = \frac{\sqrt{2ME}}{3} \delta_{\ell 1} \mathbf{e}_\mu \quad \text{for } E < U. \quad (36)$$

Here a set of orthogonal unit vectors

$$\mathbf{e}_0 = \mathbf{e}_x; \quad \mathbf{e}_{-1} = \frac{1}{\sqrt{2}}(\mathbf{e}_y + i\mathbf{e}_z); \quad \mathbf{e}_1 = \frac{1}{\sqrt{2}}(-\mathbf{e}_y + i\mathbf{e}_z)$$

has been introduced. The exact definition of the spherical harmonics is important here. The present notation follows SCHIFF (1981).

For the special case of elastic scattering, energy and momentum are conserved. Then eqs. (35) and (36) become valid for all energies. This determines the Laplace transforms

$$\begin{aligned} \overline{F}_{D, \ell, \mu}^{(0)}(s) &= U \delta_{\ell, 0} \delta_{\mu, 0} \frac{1}{s-1}; \\ \overline{\mathbf{F}}_{P, \ell, \mu}^{(0)}(s) &= \frac{\sqrt{2MU}}{3} \delta_{\ell, 1} \mathbf{e}_\mu \frac{1}{s-1/2} \end{aligned}$$

for the zero-order moments. We then find

$$F_{D,\ell,\mu}^{(n)} = \delta_{\mu 0} E \mathcal{A}_\ell^{(n)} \left(\frac{E^{2m}}{NC} \right)^n \quad (37)$$

$$\begin{aligned} F_{P,\ell,\mu}^{(n)} &= \frac{1}{3} \sqrt{2ME} e_\mu \mathcal{B}_{\ell,\mu}^{(n)} \left(\frac{E^{2m}}{NC} \right)^n \\ &+ \frac{1}{3} \sqrt{2MU} e_0 \delta_{\mu 0} \frac{\Gamma_m E}{NS(U)} \frac{1}{1/2 - 2m} \mathcal{C}_\ell^{(n)} \left(\frac{E^{2m}}{NC} \right)^{n-1} \end{aligned} \quad (38)$$

where the coefficients $\mathcal{A}_\ell^{(n)}$, $\mathcal{B}_{\ell,\mu}^{(n)}$, and $\mathcal{C}_\ell^{(n)}$ are identical with those entering the flux density, eq. (29) on page 17. Note that the freezing energy U enters only into the moments belonging to the \mathcal{C} -family and even there only as a common factor. Note that according to the criterion of significance spelled out in section 4.3 all moments with $|\mu| \geq 2$ have to be ignored.

It is seen that the family of moments determining the deposited energy is equivalent with the leading family governing the flux density, i.e., the \mathcal{A} family originating in $(n, \ell) = (0, 0)$ and shown in the upper part of table I. The deposited momentum generates two families originating in $(n, \ell) = (0, 1)$ and $(1, 0)$, respectively, corresponding to the \mathcal{B} and \mathcal{C} families in table II. However, the relative weight of the two families differs from that in the flux density. The origin of this behavior is obvious: The integrated momentum is exactly proportional to \sqrt{E} and, therefore, has the simple Laplace transform $\sim (s - 1/2)^{-1}$. On the other hand, the anisotropic term in the integrated particle flux is only asymptotically $\propto \sqrt{E}$ and its Laplace transform is $\propto 1/I_1(s)$ which is a more complex expression. This feature is immaterial to the moments in the \mathcal{B} -family which are built up on the asymptotic form of the zero'th moment, but it does affect the moments of the \mathcal{C} -family which originate in the low-energy behavior of the first moment. This difference propagates into all higher orders.

5 Depth Profiles

5.1 Approximate Expression for Flux Density

Since \mathcal{B} - and \mathcal{C} -terms enter with different weights into the moments over flux and deposited momentum, the anisotropic part of the flux density cannot just be proportional to the density of deposited momentum as has been asserted previously (SIGMUND, 1981). It is, therefore, necessary to separately consider the three distributions underlying the \mathcal{A} -, \mathcal{B} -, and \mathcal{C} -families.

It was recognized recently that the missing link is a term proportional to the gradient of the deposited energy (SCKERL ET AL., 1995). We may write the flux

density in the form

$$G(E, \mathbf{e}; W, \boldsymbol{\Omega}, x) = \frac{\Gamma_m}{4\pi NS(W)} \left[\frac{F_D(E, \mathbf{e}; x)}{W} - K_m (\boldsymbol{\Omega} \cdot \mathbf{e}_x) \frac{\partial F_D(E, \mathbf{e}; x) / \partial x}{NS(W)} + 3 \frac{\boldsymbol{\Omega} \cdot \mathbf{F}_P^0(E, \mathbf{e}; x)}{\sqrt{2MW}} \right] \quad (39)$$

where K_m is a constant to be determined. The function \mathbf{F}_P^0 is defined through its moments via eq. (38). Only the \mathcal{B} -moments contribute. \mathbf{F}_P^0 is one of two contributions making up the deposited-momentum profile, cf. eq. (42) below. The \mathcal{C} -contributions have been collected in the gradient term. Thus, \mathbf{F}_P^0 has simple scaling properties, its symmetry is governed by the direction of the incident beam, and just like F_D it is independent of U (or W). The latter feature was utilized in writing down eq. (39).

For a proof of eq. (39) all terms on the left and the right are expanded in terms of spherical harmonics and moments are taken over the depth coordinate. The resulting equation has to be satisfied separately for all (ℓ, μ) , and further separation is possible into terms proportional to $Y_{00}^*(\boldsymbol{\Omega})$, $Y_{1\mu}^*(\boldsymbol{\Omega})$, and $Y_{10}^*(\boldsymbol{\Omega})$, respectively. Terms belonging to the \mathcal{A} - and \mathcal{B} -families turn out to be identical on both sides while terms belonging to the \mathcal{C} -family become identical provided that

$$K_m = \frac{1}{(1-m)I_0(3/2-2m)} \quad (40)$$

and

$$n\mathcal{A}_\ell^{(n-1)} = \mathcal{C}_\ell^{(n)}. \quad (41)$$

Eq. (41) follows readily from eqs. (32) on page 18, and eq. (40) specifies K_m .

A slightly more complex decomposition was applied in our recent communication (SCKERL ET AL., 1995). Note in particular that the constant k_m introduced there differs from K_m as introduced above. The present form requires more caution with regard to divergent terms (as will be seen below) but makes the scaling properties more transparent.

5.2 Deposited Momentum

We may similarly decompose the density of deposited momentum into contributions from the \mathcal{B} - and \mathcal{C} -family. This yields

$$\mathbf{F}_P(E, \mathbf{e}; x, U) = -\frac{\Gamma_m}{3(1/2-2m)} \sqrt{2MU} \mathbf{e}_x \frac{\partial F_D(E, \mathbf{e}; x) / \partial x}{NS(U)} + \mathbf{F}_P^0(E, \mathbf{e}; x). \quad (42)$$

This decomposition, which has been proposed by GLAZOV (1995), is simpler than the one made in our previous note (SCKERL ET AL., 1995).

5.3 Inverse Relationships

We have now the option to insert the asymptotic expression eq. (39) into the exact relations (5) and (6) on page 9 and in this way to check the accuracy of the former. Insertion of eq. (39) into eq. (9) yields

$$G(E, \mathbf{e}; W, x) = \frac{\Gamma_m}{NS(W)} \frac{F_D(E, \mathbf{e}; x)}{W}$$

$$H(E, \mathbf{e}; W, x) = \frac{\Gamma_m}{NS(W)} \left[-\frac{1}{3} K_m \mathbf{e}_x \frac{\partial F_D(E, \mathbf{e}; x)/dx}{NS(W)} + \frac{F_P^0(E, \mathbf{e}; x)}{\sqrt{2MW}} \right].$$

Insertion into (8) and integration over the interval $U < W < E$ yields relations that are fulfilled asymptotically in the limit of $U \ll E$. The leading deviations from identity go as $(U/E)^{1-m}$.

5.4 Divergencies

Go back briefly to the first moment, $n = 1$ in eq. (29) on page 17 for $\ell = \mu = 0$. The third term in the brackets is seen to diverge for $m = 1/4$ because of the factor $I_1(1 - 2m) = I_1(1/2) = 0$ in the denominator. However, the corresponding second term contains a coefficient $\mathcal{B}_{0,0}^{(1)}$ which also becomes infinite for $m = 1/4$ because of the denominator $I_0(1/2 + 2m) = I_0(1) = 0$ in the recurrence relation eq. (32). This latter divergence has long been known (SANDERS, 1968).

It is easily seen that the two divergences cancel each other and that the sum of the two contributions is finite. This feature propagates into all higher moments that originate in these first-order moments. It is important, therefore, that for $m \simeq 1/4$ the two contributions to the moments over the particle flux that are associated with the \mathcal{B} - and the \mathcal{C} -families of moments, either are both taken into account or both neglected, dependent on their significance compared to the contribution from the \mathcal{A} -family. Since this statement applies to all moments it must also hold for the entire distribution. In other words, as long as eq. (39) is taken literally, with a uniquely defined power m , the second and third term in the brackets make up jointly the leading correction to the isotropic particle flux. If one of them is neglected the correction diverges for $m = 1/4$.

A similar statement may be made for the deposited momentum. This was first realized by ROOSENDAAL ET AL. (1982) and has been discussed recently (SCKERL ET AL., 1995; GLAZOV, 1995). Since the deposited momentum receives contributions only from the \mathcal{B} - and \mathcal{C} -families of moments, calculated momentum profiles based on the \mathcal{B} -family alone (LITTMARK & SIGMUND, 1975; GLAZOV, 1994b) are meaningful only for m significantly greater than $1/4$. Momentum deposition profiles have subsequently been evaluated with due account of both families (ROOSENDAAL

ET AL., 1982; SCKERL ET AL., 1995; GLAZOV, 1995). Meaningful and mutually consistent results were achieved for $E \gg U$. Artefacts are observed when E/U is not large: In that case more than the leading families would have to be taken into account.

Very few applications have been pointed out for the deposited-momentum profile itself (SCKERL ET AL., 1995). In fact, unlike the deposited energy which is very closely related to the damage profile, the deposited momentum has never been measured directly. On the other hand, any measurable parameter depending on cascade anisotropy must be related to deposited momentum. The question arises, therefore, which quantity should be tabulated.

From eqs. (39) and (42) we may deduce that the primary quantities are F_P^0 and $\partial F_D/\partial x$ from which other parameters, including deposited momentum if needed, can be determined. Caution is to be exerted when one of them is considered without the other. The moments over the function F_P^0 are those studied by LITTMARK (1974).

5.5 Physical Origin of the Gradient Term

It is seen from eq. (37) on page 22 that the deposited-energy profile $F_D(x)$ is determined entirely by the high-energy behavior (near E) of a collision cascade. At the same time eq. (39) is supposed to characterize the particle flux at the low-energy end (near W), but nevertheless the leading term in the spatial distribution appears to be $\propto F_D(x)$. This cannot be generally true and a straight inconsistency can easily be constructed. Indeed assume the stopping power to decrease rapidly with decreasing energy, say, power-like with m negative. Then the dominating portion of a particle trajectory stems from the motion at low energies, and low-energy recoil atoms may move over a wider depth range than outlined by the slowing-down behavior of the ion and the high-energy recoils.

On the other hand, low-energy recoils are generated in the region of high energy deposition, and their initial directions of motion are distributed approximately uniformly over the unit sphere. Therefore the flux goes predominantly from high to low energy deposition, i.e., the particle flux must contain a contribution governed by the negative gradient of F_D just as in Fourier's law of heat conduction.

A more quantitative argument may be formulated by means of the forward transport equation (18) on page 13. We consider a range of recoil energies $W \ll E$ so that the source term becomes immaterial, go over from velocity to energy-angle variables, and expand in spherical harmonics $Y_{\ell'\mu'}(\Omega)$ just as in case of the

backward equation (17). For $\mu' = 0$ we find

$$\begin{aligned} (2\ell' + 1)N \int dT & \left\{ K(W, T) G_{\ell', 0}(W, x) \right. \\ & \left. - \left[K(W + T, T) P_{\ell'}(\cos \phi') + K(W + T, W) P_{\ell'}(\cos \phi'') \right] G_{\ell', 0}(W + T, x) \right\} \\ & = -\frac{\partial}{\partial x} \left(\ell' G_{\ell'-1, 0}(W, x) + (\ell' + 1) G_{\ell'+1, 0}(W, x) \right) \end{aligned}$$

where ϕ' and ϕ'' are determined by the energy variables in case of elastic collisions. Consider the case of $\ell' = 1$. Here the right-hand side contains an isotropic contribution $\partial G_{00}(W, x)/\partial x$ which is essentially the $\partial F_D/\partial x$ term on the right-hand side of eq. (39), and a contribution that varies rapidly with angle and may be neglected as a first approximation. The left-hand side contains three terms which all contain $G_{10}(W, x)$, i.e., a contribution related to the third term on the right-hand side of eq. (39). Approximating $G_{10}(W, x)$ by the appropriate power law in W makes it possible to evaluate the integral and construct a quantitative connection. However, the essential conclusion is that the gradient term originates in the low-energy behavior of the cascade and will have the form given in eq. (39) for a wide variety of initial conditions.

6 Generalizations

Eq. (39) on page 23 has been written in a form that suggests it to be more general than what can be inferred from the actual derivation. It is the purpose of the present section to document that this is indeed true and to provide guidelines for how corrections can be made for physical effects which were not included above.

6.1 Non-Selfbombardment

Consider first the important case of a monoatomic medium bombarded by an arbitrary ion with an arbitrary mass. The backward transport equation for this case is a straight generalization of eq. (18) on page 13,

$$N \int d\sigma_0(\mathbf{v}; \mathbf{v}', \mathbf{v}'') \left\{ G_0(\mathbf{v}) - G_0(\mathbf{v}') - G(\mathbf{v}'') \right\} + \cos \Theta \frac{\partial}{\partial x} G_0(\mathbf{v}) = 0 \quad (43)$$

where the subscript 0 denotes the foreign ion. It is important to note that this subscript is missing in the recoil term under the integral which takes over the role of a source term. A source term of the form present in eq. (18) does not occur since no target atoms are moving initially.

Now assume the ion-target cross section $d\sigma_0$ to have power form. We may then solve eq. (43) by Laplace transform. This yields the following result for the zero-order moments,

$$\overline{G}_{0;\ell,\mu;\ell',\mu'}^{(0)}(s) = \frac{K_\ell(s)}{J_\ell(s)} \overline{G}_{\ell,\mu;\ell',\mu'}^{(0)}(s) \quad (44)$$

where

$$J_\ell(s) = \int_0^\gamma dt t^{-1-m} \left\{ 1 - P_\ell(\cos \phi')(1-t)^s \right\} \quad (45)$$

$$K_\ell(s) = \int_0^\gamma dt t^{-1-m} P_\ell(\cos \phi'') t^s. \quad (46)$$

Here, γ is the energy-transfer factor defined after eq. (24). The additional subscript 0 indicates the incident particle, and $\cos \phi'$ and $\cos \phi''$ have been specified in eq. (28) on page 15. Eq. (44) is remarkable since it does not imply assumptions about $\overline{G}_{\ell,\mu;\ell',\mu'}^{(0)}(s)$ except that it exists. In particular no assumption enters regarding the relation between the power cross section $d\sigma_0$ and the cross section $d\sigma$ governing target-target interactions.

For elastic collisions we know that $\overline{G}_{\ell,\mu;\ell',\mu'}^{(0)}(s)$ has its leading singularities in $s = 1$ for $\ell = 0$ and in $s = 1/2$ for $\ell = 1$. It is easily verified that

$$\frac{K_0(1)}{J_0(1)} = 1 \text{ and } \frac{K_1(1/2)}{J_1(1/2)} = \sqrt{\frac{M_0}{M}}$$

where M_0 and M denote ion and target mass, respectively. Therefore, within the approximation adopted in this paper we have

$$\begin{aligned} G_{0;0,0;0,0}^{(0)}(E; W) &= G_{0,0;0,0}^{(0)}(E; W) \\ G_{0;1,\mu;1,\mu}^{(0)}(E; W) &= \sqrt{\frac{M_0}{M}} G_{1,\mu;1,\mu}^{(0)}(E; W) \end{aligned} \quad (47)$$

independent of the scattering law since $J_\ell(s)$ is nonvanishing for $s > 0$. These two terms, which generate the \mathcal{A} and \mathcal{B} families of moments, are thus governed entirely by target properties except that the factor $\sqrt{M_0/M}$ needs to be taken care of properly. This may be done by replacing the factor $\sqrt{E/W}$ in eq. (29) by $\sqrt{2M_0E/2MW}$, i.e., the ratio of momenta.

The third term in the brackets of eq. (29) on page 17 does not have a form that would suggest a dependence on ion mass. Indeed the Laplace transform $\overline{G}_{0;0,0;1,0}^{(1)}(s)$ is given by

$$\overline{G}_{0;0,0;1,0}^{(1)}(s) = \frac{1}{J_0(s)} \left[K_0(s) \overline{G}_{0,0;1,0}^{(1)}(s) + \frac{W^{2m}}{NC_0} \overline{G}_{0;1,0;1,0}^{(0)}(s - 2m) \right]$$

where C_0 denotes the constant in the power cross section for ion-target interaction². Here only the first term in the brackets yields a singularity at $s = 1$. Consequently we have

$$\overline{G}_{0;0,0;1,0}^{(1)}(s \simeq 1) = \overline{G}_{0,0;1,0}^{(1)}(s \simeq 1)$$

as was asserted above.

An analogous analysis may be performed for deposited energy and momentum with M being replaced by M_0 in the normalization condition (22), page 14. Similar to eq. (47) we find

$$\begin{aligned} F_{D,0;0,0}^{(0)} &= F_{D,0,0}^{(0)} \\ \mathbf{F}_{P,0;1,\mu}^{(0)} &= \sqrt{\frac{M_0}{M}} \mathbf{F}_{P,1,\mu}^{(0)}. \end{aligned} \quad (48)$$

With our decomposition into three significant families it is clear that the higher moments for each family apply to flux as well as deposited energy and momentum.

From eq. (48) we may conclude that eq. (39) on page 23 equally well applies to non-selfbombardment provided that proper beam-dependent deposited-energy and momentum distributions are employed.

6.2 Electronic Stopping: High-Energy Correction

This is the first of two paragraphs providing modifications to the central relationships when electronic stopping is not negligible. We shall treat the effect within the traditional scheme (LINDHARD ET AL., 1963a, 1963b) outlined already in section 2.5 on page 10,

- separation of collisions into electronic and nuclear events,
- neglect of angular deflection in electronic collisions, and
- neglect of any feeding of energy from the electronic into the nuclear system.

For self-bombardment an additional term

$$(2\ell + 1)NS_e(E) \frac{\partial}{\partial E} G_{\ell,\mu;\ell',\mu'}^{(n)}(E; W) \quad (49)$$

appears in eq. (23) (page 14) on the left-hand side, and corresponding terms have to be inserted in eq. (34) (page 21) and the equivalent set of moment equations for deposited momentum. Here $S_e(E)$ is the electronic stopping cross section.

The primary effect of electronic stopping is a draining of energy at all stages of a collision cascade. Therefore neither energy nor momentum are conserved as

²This notation interferes with SIGMUND (1969b) where C_0 denotes the value of C_{ij} for $m = 0$. The quantity called C_0 here was denoted $C_{(1)}$ in earlier work (WINTERBON ET AL., 1970).

far as nuclear motion is concerned. In particular the normalizing integral over the deposited energy F_D becomes proportional to a function $\nu(E)$ representing the part of the initial energy E which ends up in nuclear motion (LINDHARD ET AL., 1963a). This function is well-defined provided that S_e/S_n becomes small at low energies. Also the zero'th moment over the flux density for $\ell = 0$ becomes $\propto \nu(E)$ under the same assumption.

The assumption underlying this treatment is that $\nu(E)$ becomes $\propto E$ at low energies. In case of non-negligible electronic stopping at low energies, the proportionality factor will differ from the one valid for elastic scattering. That effect will be considered in section 6.4.

A rough estimate demonstrates the effect of electronic stopping on the zero'th moment over the deposited-momentum profile, i.e., moments over momentum or flux containing $B_{1\mu}^{(0)}$, to be given by the substitution $\sqrt{E} \rightarrow \sqrt{\nu(E)}$. This relation – which is not exact – may be rationalized by means of an approximation mentioned by LINDHARD ET AL. (1963a): Consider first the integral equation for $\nu(E)$,

$$N \int d\sigma_n \left\{ \nu(E) - \nu(E-T) - \nu(T) \right\} + NS_e(E) \frac{d\nu(E)}{dE} = 0.$$

Utilizing the fact that the cross section for nuclear scattering $d\sigma_n$ peaks at small recoil energies T , one may approximate $\nu(T) \simeq T$ and $\nu(E-T) \simeq \nu(E) - T d\nu(E)/dE$. This yields the well-known estimate

$$\nu(E) \simeq \int_0^E dE' \frac{S_n(E')}{S(E')},$$

where $S = S_n + S_e$. When the same approximations are applied to any of the three components of the deposited momentum, say $P(E)$, one finds

$$P(E) \simeq \sqrt{2M} \int_0^E dE' \frac{S_n(E')}{S(E')\sqrt{E'}} \exp \left(- \int_{E'}^E dE'' \frac{S_n(E'')}{2E''S(E'')} \right).$$

This expression is easily seen to reduce to $\sqrt{2ME}$ when electronic stopping is neglected, as it should.

For a convenient estimate assume that

$$\frac{S_n(E)}{S(E)} = 1 - \left(\frac{E}{E_1} \right)^r; \quad E < E_1 \text{ and } r > 0;$$

Then integration yields

$$\nu(E) = E \left[1 - \frac{1}{r+1} \left(\frac{E}{E_1} \right)^r \right]$$

and

$$P(E) = \sqrt{2ME} \left[1 - \frac{1}{2(r+1)} \left(\frac{E}{E_1} \right)^r \dots \right]$$

by Taylor expansion for $E \ll E_1$. This confirms the above assertion.

6.3 Role of Binding

Binding forces to lattice sites may be modelled by incorporation of a binding energy U_b in the recoil term of transport equations (LINDHARD ET AL., 1963a). This implies the substitution $E'' = T - U_b$ in eq. (23) on page 14 and complicates the algebra involved in the Laplace transform method. However, series expansion in powers of U_b/W has been demonstrated to lead to valid asymptotic solutions (ANDERSEN & SIGMUND, 1974).

In brief, the Laplace transform of the recoil term contributing to eq. (26) changes from $\overline{G}_{\ell,\mu;\ell',\mu'}^{(n)}(s)K_\ell(s)$ to

$$K_\ell(s) \int_0^\infty du e^{-su} G_{\ell,\mu;\ell',\mu'}^{(n)}(u) \left(1 + \frac{U_b}{W} e^{-u} \right)^{-s-1},$$

where $K_\ell(s)$ is the function defined by eq. (46) for $\gamma = 1$. After Taylor expansion of the above integral in powers of U_b/W as well as of $\overline{G}_{\ell,\mu;\ell',\mu'}^{(n)}(s)$ itself,

$$\overline{G}_{\ell,\mu;\ell',\mu'}^{(n)}(s) = \sum_\nu \overline{G}_{\ell,\mu;\ell',\mu';\nu}^{(n)}(s) \left(\frac{U_b}{W} \right)^\nu,$$

the resulting system of equations may be solved recurrently starting from the zero-binding solution $\nu = 0$. It is then readily seen that all coefficients $\overline{G}_{\ell,\mu;\ell',\mu';\nu}^{(n)}(s)$ are singular at $s = s_0$ where

$$s_0 = \begin{cases} 1 & \text{for } \ell = 0 \\ 1/2 & \text{for } \ell = 1 \end{cases}$$

and, therefore, contribute to the asymptotic solution for $E \gg W > U_b$. The first few terms may be conveniently expressed by their ratios to the solution for vanishing binding,

$$\begin{aligned} \frac{G_{\ell,\mu;\ell,\mu;1}^{(0)}(E)}{G_{\ell,\mu;\ell,\mu;0}^{(0)}(E)} &= -(s_0 + 1) \frac{K_\ell(s_0)}{I_\ell(s_0 + 1)} \\ \frac{G_{\ell,\mu;\ell,\mu;2}^{(0)}(E)}{G_{\ell,\mu;\ell,\mu;0}^{(0)}(E)} &= (s_0 + 1)(s_0 + 2) \frac{K_\ell(s_0)}{I_\ell(s_0 + 2)} \left(\frac{1}{2} + \frac{K_\ell(s_0 + 1)}{I_\ell(s_0 + 1)} \right), \end{aligned}$$

where $J_\ell(s)$ is the function defined by eq. (45) for $\gamma = 1$.

With this we find that the $n = 0$ moment of the \mathcal{A} -family receives a correction factor

$$1 - (2 - m) \frac{U_b}{W} + (2 - m)^2 \left(\frac{U_b}{W} \right)^2 \cdots \simeq \frac{1}{1 + (2 - m)U_b/W}. \quad (50)$$

This result was derived long ago (SIGMUND, 1973). URBASSEK ET AL. (1995) rederived it recently and confirmed its accuracy by computer simulation. They also pointed out an inconsistency with a later, less accurate approximation to the same series (SIGMUND, 1981).

Corrections to moments for $n \geq 1$ are of the order of U_b/E and are thus negligible within a scheme where only the two leading terms in E/W are analysed. Therefore we may conclude that the factor written up in eq. (50) also applies to the profile belonging to the \mathcal{A} -family and not just to the moments.

The modifications on moments and profiles of the \mathcal{B} -family are evaluated similarly. They are accomplished by a factor

$$1 - \frac{3}{4}(2 - m) \frac{U_b}{W} + \frac{5}{8}(2 - m)^2 \left(\frac{U_b}{W} \right)^2 \cdots \simeq \left(1 + \frac{11}{12}(2 - m) \frac{U_b}{W} \right)^{-9/11}.$$

As in eq. (50), the binomial approximation is exact to the second order in U_b/W . Within the accuracy of the scheme this expression looks sufficiently similar to eq. (50) to justify ignoring the difference.

The effect on the gradient term, i.e., the \mathcal{C} -family, is more complex since binding corrections enter twice. Since these terms are proportional to $\overline{G}_{1,0;1,0}^{(0)}(s)$, a \mathcal{B} -type correction enters but taken at $s = 1 - 2m$ instead of $s_0 = 1/2$. That correction may be written in the form

$$R = 1 - (2 - 2m) \frac{K_1(1 - 2m)}{I_1(2 - 2m)} \frac{U_b}{W} \cdots \quad (51)$$

In addition, another correction enters which is of the \mathcal{A} type and results from the singularity of $\overline{G}_{0,0;1,0}^{(1)}(s)$ at $s = 1$. That correction has exactly the form of eq. (50).

Examination of eq. (51) reveals that this correction goes in the same direction as all other ones discussed, but that it varies more rapidly with m . For $m = 0$ it has about half the magnitude indicated by eq. (50) but it approaches infinity at $m = 1/2$. While the value of m in the pertinent energy range is well below that limit we do keep in mind that the binding correction is more pronounced in the gradient term than in the energy and momentum terms. This may be not too surprising in view of the origin of this term in the motion of low-energy particles.

6.4 Electronic Stopping: Low-Energy Correction

This paragraph serves a study of the effect of electronic stopping on the low-energy behavior of a cascade. A similar procedure as the one presented in the preceding section can be applied to estimate the contribution of electronic stopping to the $S(W)$ denominators in eq. (39). We recall that this notation is just an abbreviation for $S_n(W)$ since electronic stopping was neglected in the derivation. A physical argument (SIGMUND, 1981) generates a factor $1/NS(E)$ from the energy degradation $dE/dt = v dE/dx$. The nature of the stopping process is immaterial in this argument. Therefore, $NS(W)$ ought to be the total (nuclear plus electronic) stopping power. Yet it is more doubtful whether a similar argument holds for the additional denominator $1/NS(W)$ in the C term.

Assume some power dependence of the electronic stopping cross section,

$$S_e(E) = kE^\alpha$$

with $\alpha < 1$, and add eq. (49) on page 28 to eq. (23) on page 14. In Laplace space this implies addition of a term

$$(2\ell + 1) \frac{NS_e(W)}{W} (s - \alpha + 1) \overline{G}_{\ell, \mu; \ell', \mu'}^{(n)}(s - \alpha + 1)$$

in eq. (26). Then, recurrent solution is possible by Taylor expansion in the ratio between electronic and nuclear stopping power at energy W . With the parameter

$$\varepsilon = \frac{NS_e(W)}{NCW^{1-2m}},$$

the procedure outlined above yields series expressions for the correction factors to be applied to the three contributions to the particle flux derived for elastic collisions. For the \mathcal{A} -family we obtain

$$R_{\mathcal{A}} = 1 + \sum_{j=1}^{\infty} (-\varepsilon)^j \prod_{r=1}^j X_0 \left(1 + r(1 - \alpha) \right),$$

where

$$X_\ell(s) = \frac{s}{I_\ell(s)}.$$

This series is divergent but offers itself to transformation into a continued fraction. We refrain from going through the explicit procedure but approximate the result by taking into account only the first term, so that

$$R_{\mathcal{A}} \simeq \frac{1}{1 + \varepsilon X_0(2 - \alpha)}. \quad (52)$$

For the \mathcal{B} -family the same procedure leads to

$$R_{\mathcal{B}} \simeq \frac{1}{1 + \varepsilon X_1(3/2 - \alpha)}. \quad (53)$$

As in the previous section, the \mathcal{C} -family receives two correction terms. This matches very well the occurrence of two denominators $S(W)$ in eq. (39) in that term. The first factor $R_{\mathcal{C},1}$ is identical with $R_{\mathcal{A}}$ specified in eq. (52), while the second follows from eq. (53) by the replacement $1/2 \rightarrow 1 - 2m$, i.e.,

$$R_{\mathcal{C},2} \simeq \frac{1}{1 + \varepsilon X_1(2 - 2m - \alpha)}. \quad (54)$$

We note that the chosen representation of the correction factors is consistent with the expectation that one or several of the denominators in eq. (39) expand according to $S(W) \rightarrow S_n(W) + S_e(W)$. The actual expansions take on the form

$$S(W) \rightarrow S_n(W) + \frac{X}{1 - m} S_e(W),$$

where X represents the proper expression occurring in the above three correction factors.

Numerical evaluation of eqs. (52-52) shows that $X/(1-m)$ exceeds the expected lower bound $X/(1-m) = 1$ for all feasible values of m and α . The excess is moderate – $X/(1-m) < 2$ – for eqs. (53) and (54) but somewhat greater in case of the energy – $X/(1-m) \lesssim 3$.

The role of electronic stopping at low energies was studied many years ago but never published (WINTERBON & SIGMUND, 1973). The problem has also been discussed in context with computer simulations (BIERSACK & ECKSTEIN, 1984; HARRISON & JAKAS, 1984, 1985).

6.5 More General Cross Sections

The form of eq. (39) (page 23) also suggests that the power cross section need not be a necessary basis. It has already been argued in section 4.4 (page 19) that in applications we may be forced to operate with two power cross sections applying to the range around the initial energy E and a recoil energy W , respectively. With W varying from somewhat below E – wherever the asymptotic expression for $E/W \gg 1$ may start to be meaningful – downward, the second m -value may vary considerably.

The guiding principle in the notation underlying eq. (39) and its various analogs is that explicit occurrences of m should be condensed into dimensionless numbers, here Γ_m and K_m , where Γ_m is a well-established parameter that determines the

sharing of energy between collision events above and below threshold (SIGMUND, 1969c). Γ_m varies slowly in the interval $0 < m < 1$ (figure 1). On the other hand the quantity K_m , although varying slowly for $0 < m \lesssim 0.2$, becomes singular at $m = 1/4$. This is not influential for the flux density because the singularity is cancelled by a corresponding one with the opposite sign in the third term in eq. (39).

6.6 Isotope Effect

The present paragraph serves to provide an estimate of the particle flux for a medium containing particles with different masses. This case is of interest in the study of isotope effects. This aspect has been studied long ago for the isotropic contribution to the particle flux (ANDERSEN & SIGMUND, 1974) and more recently for the momentum term (SIGMUND & SCKERL, 1993). We shall rederive those results here, but the main goal is an estimate of the mass dependence of the gradient term.

The general formalism has been outlined in appendix A. While the expressions governing absolute fluxes may look a bit clumsy, their ratios reduce to fairly transparent expressions. In the notation of appendix A we find the following expressions for the ratios between particle fluxes of isotopes 1 and 2 in a binary mixture,

$$\begin{aligned} P_A &= \frac{\Sigma''_{21,0}(1)}{\Sigma''_{12,0}(1)} \\ P_B &= \frac{\Sigma''_{21,1}(1/2)}{\Sigma''_{12,1}(1/2)} \\ P_C &= \frac{\Sigma''_{21,0}(1)\overline{G}_{11;10;10}^{(0)}(1-2m) + \Sigma''_{12,0}(1)\overline{G}_{21;10;10}^{(0)}(1-2m)}{\Sigma''_{21,0}(1)\overline{G}_{12;10;10}^{(0)}(1-2m) + \Sigma''_{12,0}(1)\overline{G}_{22;10;10}^{(0)}(1-2m)} \end{aligned}$$

which, according to eqs. (71) and (72) and the integrals (45, 46) reduce to

$$P_A = \frac{N_1 C_{21}}{N_2 C_{12}} \quad (55)$$

$$P_B = \frac{N_1 C_{21} J_{21,1}(1/2)}{N_2 C_{12} K_{12,1}(1/2)} \quad (56)$$

$$P_C = \frac{N_1 C_{21} N_1 C_{21} J_{21,1} + N_2 C_{22} I_1 + N_2 C_{12} K_{21,1}}{N_2 C_{12} N_2 C_{12} J_{12,1} + N_1 C_{11} I_1 + N_1 C_{21} K_{12,1}} \Big|_{s=1-2m} \quad (57)$$

Here, $I(s) = J(s) - K(s)$, and the first two subscripts in $J_{ik,\ell}(s)$ and $K_{ik,\ell}(s)$ denote the collision partners.

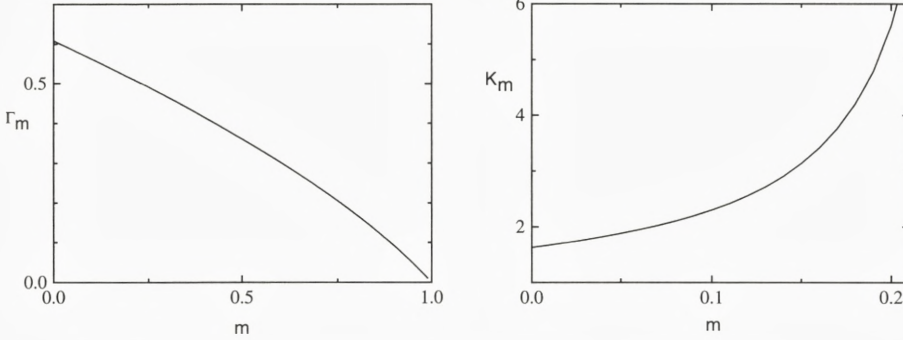


Figure 1: The constants Γ_m , eq. (30) and K_m , eq. (40) versus m .

It is seen that the well-known isotope effect in the isotropic flux (ANDERSEN & SIGMUND, 1974), expressed by the ratio

$$\frac{N_1 C_{21}}{N_2 C_{12}} = \frac{N_1}{N_2} \left(\frac{M_2}{M_1} \right)^{2m} \quad (58)$$

by insertion of eq. (25), is common to all flux ratios. The additional factor in eq. (56) is readily seen to reduce to $\sqrt{M_1/M_2}$, a result found previously (SIGMUND & SCKERL, 1993). Thus, the isotope effect in the \mathcal{B} -term,

$$P_{\mathcal{B}} = \frac{N_1}{N_2} \left(\frac{M_1}{M_2} \right)^{1/2-2m} \quad (59)$$

is typically preferential in the heavier species, provided that $m < 0.25$ at the energy W where the flux is recorded.

The flux ratio for the \mathcal{C} -family is evaluated conveniently in the limit of small isotopic differences. Up to first order we find

$$P_{\mathcal{C}} \simeq \frac{N_1}{N_2} \left(\frac{M_2}{M_1} \right)^{2m} \left(1 + \frac{M_1 - M_2}{M} Z(m) \right) \quad (60)$$

where

$$Z(m) = \frac{\Delta J_1(1-2m) - m I_1(1-2m)}{J_1(1-2m)} \quad (61)$$

and

$$\Delta J_1(s) = \frac{1}{2} \int_0^1 dt t^{-m} (1-t)^{s-1/2}.$$

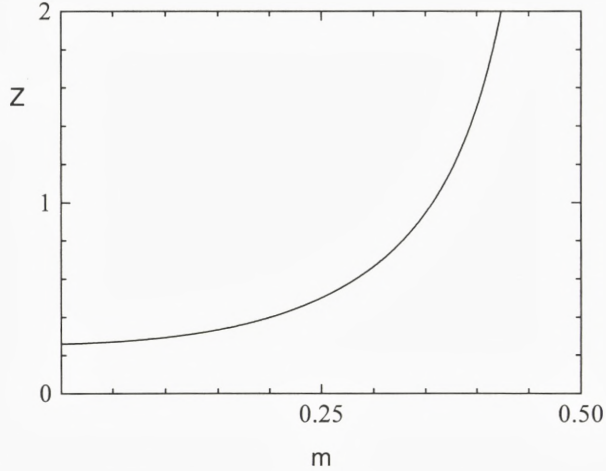


Figure 2: The function $Z(m)$ defined by eq. (61)

The function $Z(m)$ is shown in figure 2. It is seen to be positive in the pertinent range of m -values and surprisingly large. Most notably, the gradient term prefers the heavy species, as does the momentum term.

7 Results

7.1 Moments

Moments were evaluated recurrently following the procedure described by WINTERBON ET AL. (1970). Numerical values were checked against those reported by WINTERBON ET AL. (1970) for deposited energy and LITTMARK (1974) for deposited momentum, and excellent agreement has been found.

7.2 Construction of Profiles

Profiles reported here have been evaluated by the Padé method (LITTMARK, 1974). Consider some profile $f(\xi)$ and write down its Fourier transform

$$\hat{f}(\tau) = \frac{1}{2\pi} \int_{-\infty}^{\infty} d\xi e^{-i\xi\tau} f(\xi) = \frac{1}{2\pi} \sum_{n=0}^{\infty} \frac{(-i\tau)^n}{n!} f^{(n)}$$

as a Taylor series in the moments $f^{(n)}$ over $f(\xi)$. With a finite number of moments given, the Fourier transform can be approximated by a polynomial. The polynomial is then matched by a Padé approximant,

$$\hat{f}(\tau) \simeq \frac{p_r(\tau)}{q_s(\tau)},$$

where $p_r(\tau), q_s(\tau)$ each are polynomials of degree r, s , respectively, with $s > r$. Inverse Fourier transforms of the resulting Padé approximants have been found numerically.

In view of the number of coefficients determining the polynomials in eq. (7.2) we need $r + s + 1$ moments. Criteria for the choice of r and s have been discussed by LITTMARK (1974). In the numerical procedure great care has been taken to find stable solutions for Padé approximants. Typically this required taking into account moments of order up to $n = 20$, but accurate solutions were in particular cases found already with $n = 6$ to 8. Profiles presented here were mostly evaluated with one of Littmark's favored choices, $r = 6$ and $s = 10$.

The Padé method tends to smear out discontinuities which may be present at $x = 0$. Such discontinuities may be dramatic when the lower energy limit W or U is set equal to zero (GLAZOV, 1994a, 1994b), and they originate in the fact that dissipation of energy/momentum starts in the plane $x = 0$. In particular, such discontinuities are unrelated to the possible presence of a target surface, although a surface, if present in $x = 0$, must be suspected to substantially modify them. The results to be reported below always refer to nonvanishing values of W or U . This feature is common with the solutions offered in our previous work (SCKERL ET AL. 1995) as well as a recent paper by GLAZOV (1995).

7.3 Monte Carlo Simulation

As an independent check also Monte Carlo simulations were performed. A program was developed for this specific purpose based on an existing code (VICANEK & URBASSEK, 1988). The code was geared to simulate the physical situation in accordance with the theoretical model described above, i.e., random motion in an infinite medium, characterized by a scattering law equivalent with eq. (24) and with a cutoff impact parameter large enough to ensure a negligible systematic error. Deposited-momentum and -energy profiles were determined in accordance with an adopted threshold U and a depth resolution equivalent with a grid of typically 100 intervals.

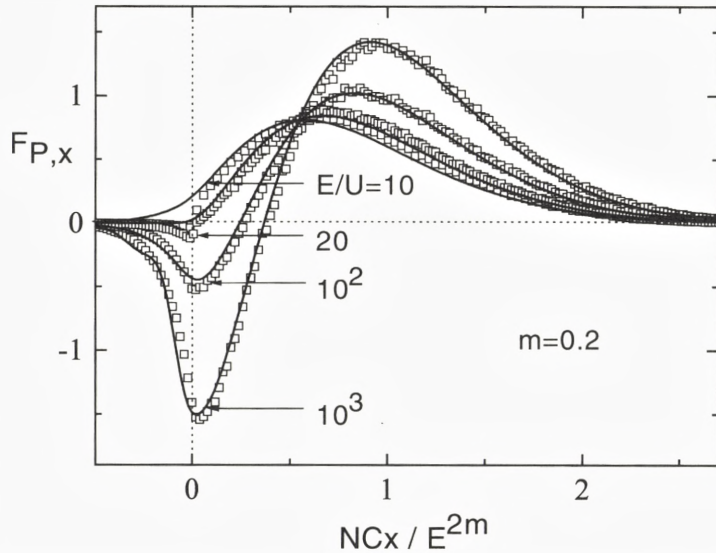


Figure 3: Deposited-momentum profiles for self-bombardment at normal incidence, calculated from the \mathcal{B} - and \mathcal{C} -families for four values of E/U and power-law scattering neglecting electronic stopping with $m = 0.2$. Circles found by Monte Carlo simulation of 40 000 events. Lines found by Padé method on the basis of ten moments. The abscissa unit is E^{2m}/NC . Profiles have been normalized to unity.

7.4 Deposited Momentum and Energy

Figure 3 shows deposited-momentum profiles for self-bombardment at normal incidence, calculated from the \mathcal{B} - and \mathcal{C} -families for four values of E/U and power-law scattering neglecting electronic stopping with $m = 0.2$. It is seen that there is nearly perfect agreement between the Monte Carlo results and the profiles reconstructed by the Padé method, also near the ‘surface’ $x = 0$. The only exception occurs in the behavior around $x \simeq 0$ for $E/U = 10$. Here the asymptotic solution predicts an inward-directed momentum for $x < 0$ which is unphysical. This limitation of the asymptotic approximation is, of course, not found in the Monte Carlo solution which turns negative also for this comparatively low value of E/U .

According to GLAZOV (1995), the momentum deposition profile makes a jump at the surface, the magnitude of which is $\sim (U/E)^{1-m}/(1-m)$ for $E \gg U$ in the units applied in figure 3. This becomes ~ 0.2 at the lowest ratio, $E/U = 10$. Within the grid chosen for the Monte Carlo computations this value is compatible with the simulation data.

Figure 4 shows similar results for $m = 1/3$. This case was considered by

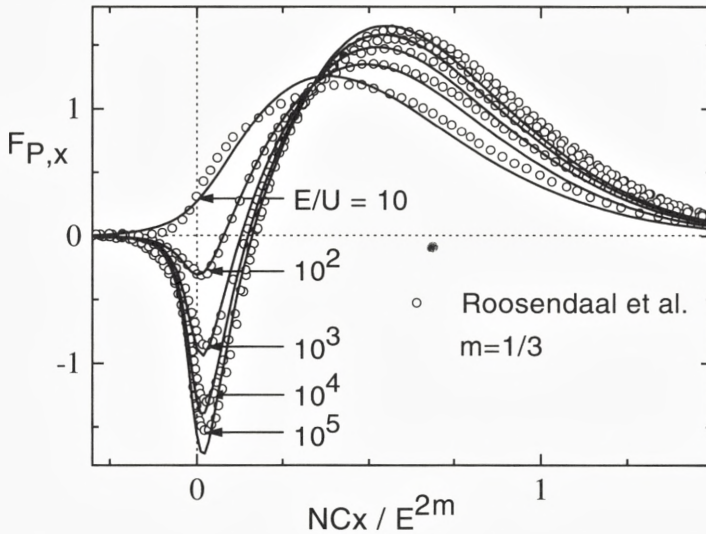


Figure 4: Same as figure 3 for five values of E/U and $m = 1/3$. Compared with results reported by ROSENDAAL ET AL., 1982.

ROSENDAAL ET AL. (1982) and we find surprisingly close agreement, considering that their expansion scheme for moments differed from ours. Their profiles were also constructed by the Padé method. Again the curve for $E/U = 10$ shows an unphysical behavior at $x < 0$ where it is still positive, as pointed out also by GLAZOV (1995).

Figure 5 shows similar profiles for three different power cross sections. It is seen that for $m = 0.4$ the momentum profile is insensitive to the ratio E/U except near $x = 0$ while for $m = 0.2$ all parts of the profile are sensitive to E/U . The latter feature, as well as the qualitative behavior of the profile is in good agreement with what was found by GLAZOV (1995) for $m = 1/6$. The procedure utilized in that work to construct profiles is expected to be more reliable near $x = 0$ than the Padé method. Even though the m -values differ, GLAZOV'S profiles are noticeably sharper around $x = 0$ than ours. On the other hand, the agreement with the Monte Carlo simulations indicated in figure 3 suggests that significant disagreement must be limited to a region of the order of the grid size in the simulations, i.e., 1-2% of the mean range.

The most pronounced feature emerging from figure 5 is a strong increase of the negative-momentum portion around $x = 0$ with decreasing m , i.e., with increasing importance of wide-angle deflection and, hence, momentum reversal events. This

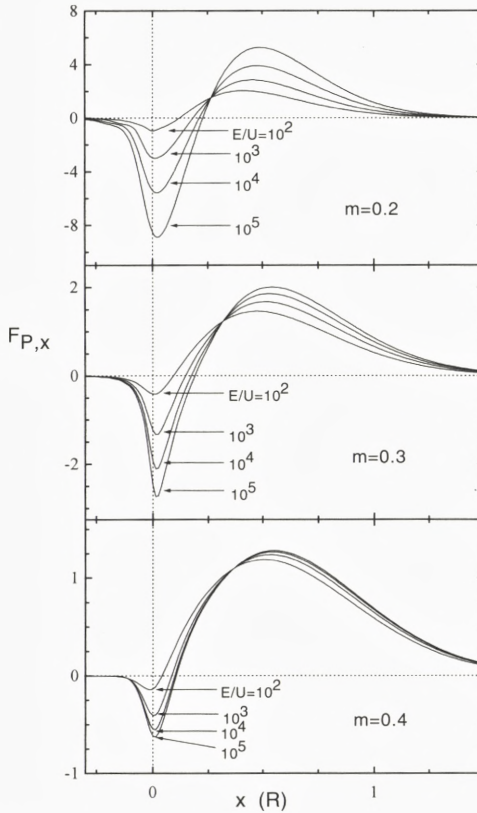


Figure 5: Deposited-momentum profiles for self-bombardment at normal incidence, calculated from the B - and C -families for four values of E/U and power-law scattering neglecting electronic stopping with $m = 0.2, 0.3$, and 0.4 . The abscissa unit is the mean pathlength of the incident particle, $R = (1 - m)E^{2m}/2mNC$. Profiles normalized to unity. Note the different ordinate scales.

feature also shows up when the mass of the bombarding ion differs from that of the target, as is illustrated in figures 6 and 7. The variation with mass ratio is very pronounced; note the different ordinate scales. Figure 6 also compares the profile of deposited energy with that of the lateral component of deposited momentum. That component is nonvanishing for oblique bombardment. It is seen that although the two profiles have similar symmetry they are by no means identical. Their relative proximity to the surface appears to be governed by the mass ratio.

7.5 Flux Density

Figure 8 shows angular distributions of the density of particle flux at different depths, i.e., the angular dependence of the quantity G , suitably normalized. Note in particular that the flux through a plane ($x = \text{const}$) carries an additional factor $|\cos \theta| = |\boldsymbol{\Omega} \cdot \mathbf{e}_x|$.

Several features emerge from a comparison of figures 8 and 9. Consider first

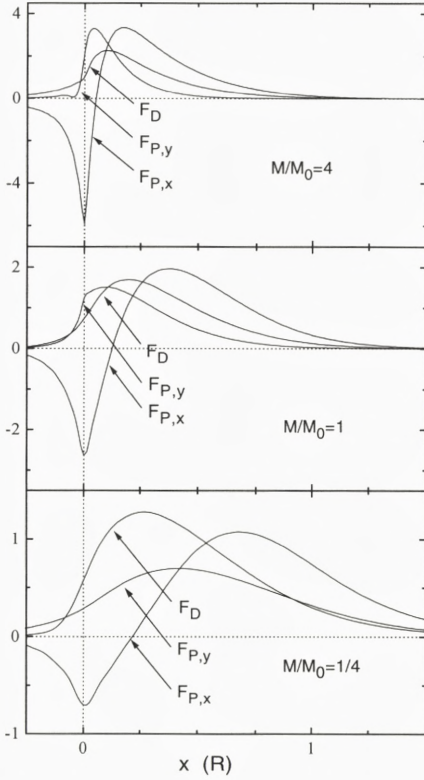


Figure 6: Deposited-energy and momentum profiles at 45° incidence for $E/U = 1000$ and mass ratios $M/M_0 = 4, 1,$ and 0.25 . Both the longitudinal (x) and the lateral (y) component of the deposited momentum are given with the y axis lying in the plane of incidence. Power scattering neglecting electronic stopping with $m = 0.3$. The abscissa unit is the mean path length of the ion, $R = (1 - m)E^{2m}/2mNC_0$. Profiles normalized to $1/\sqrt{2}$. Note the different ordinate scales.

column 3 in either graph, referring to the flux at the mean depth of deposited energy, $\langle x \rangle_D$, i.e., near the region of maximum flux density. An inward-directed correction to the particle flux is observed in all cases, depending on the energy ratio E/W but insensitive to the power exponent m and only weakly dependent on mass ratio M/M_0 . The relative magnitude of the correction, on the other hand, appears noticeable: At $E/W = 100$ the forward flux is approximately twice as large as the backward flux, yet at $E/W \gtrsim 10^3$ the difference is insignificant.

Consider next columns 4 referring to the far edge of the flux profile, $x = \langle x \rangle_D + \Delta x_D$, where Δx_D denotes the standard deviation of the damage profile in the notation of WINTERBON ET AL. (1970). Here a pronounced inward-directed flux had to be expected and is indeed found: At $E/W = 100$ the ratio between forward and backward flux is of the order of 3-4 and quite insensitive to both m and mass ratio.

Column 2 shows equivalent information at the near edge of the flux profile, $x = \langle x \rangle_D - \Delta x_D$. With the exception of the case of $m = 0.3, M/M_0 = 4$, this

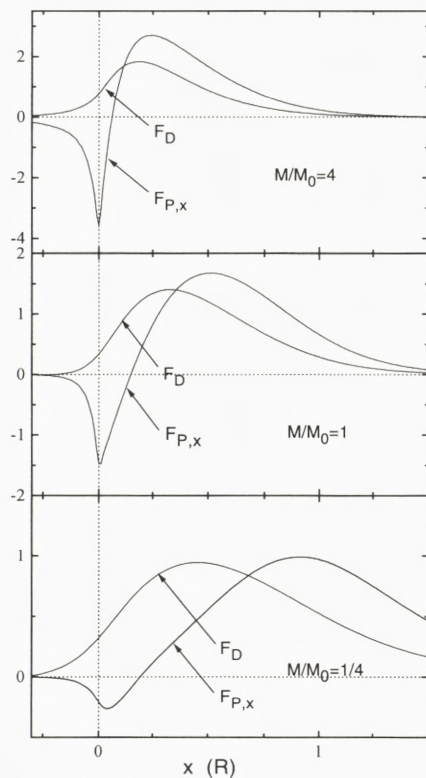


Figure 7: Same as figure 6 for normal incidence. There is no lateral momentum deposition profile in this case. Profiles normalized to 1. Note the different ordinate scales.

position appears to be close to the point of vanishing flux correction.

Finally, column 1 refers to the position $x = 0$, i.e., the plane of incidence of the primary particle where discontinuities have to be coped with and where the deposited-momentum profile is negative. We may note that for the range of mass ratios under consideration the position $x = 0$ is always to the left of $x = \langle x \rangle_D - \Delta x_D$. Thus, whenever the flux is noticeably anisotropic the anisotropy is more pronounced in column 1 than in column 2. The degree of anisotropy is very sensitive to the mass ratio. A dependence on m is visible but less pronounced. Most striking is the weak anisotropy found for $M/M_0 = 0.25$, i.e., for a heavy primary ion incident on a light target. The pronounced backward orientation of the flux for equal masses and $M/M_0 = 4$ must be caused by momentum reversal due to wide-angle scattering. Its absolute magnitude may be subject to some uncertainty because of our use of Padé approximants. Moreover, the pronounced heart shape found for $m = 0.3$ and equal masses demonstrates that the flux correction has roughly equal magnitude as the isotropic term. Therefore, subsequent correction

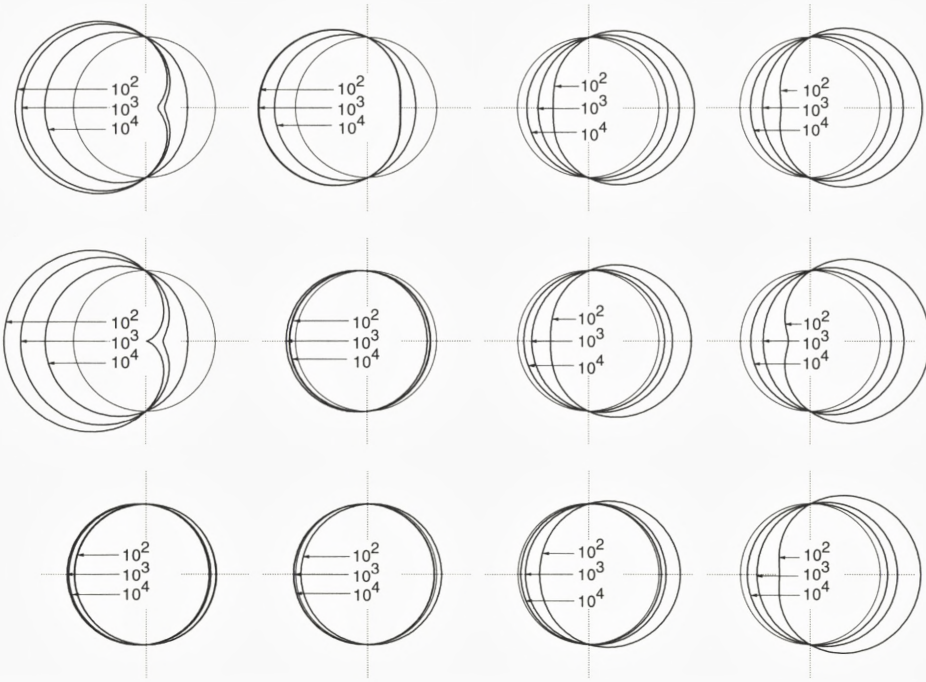


Figure 8: Angular dependence of particle flux density eq. (39) at depths $x = 0$, $\langle x \rangle_D - \Delta x_D$, $\langle x \rangle_D$, and $\langle x \rangle_D + \Delta x_D$ from left to right, for $m = 0.3$ and mass ratios $M/M_0 = 4$, 1, and 0.25 from top to bottom. Ratios E/W indicated in graphs.

terms must be suspected to have some significance. Nevertheless the tendency is clear: The flux is directed outward at all ratios E/W , and most pronouncedly so at the lower values, $E/W \sim 100$.

The fact that the anisotropy appears more pronounced for equal masses than for $M/M_0 = 4$, despite a pronouncedly higher momentum reversal in the latter case emerging from figure 6 must be due to the fact that the flux at equal masses also contains the reflected fraction of incident particles.

Figure 10 shows angular distributions of the flux density at oblique incidence. It is seen that the effect of momentum conservation is very pronounced at the far edge of the flux profile (column 4) for all mass ratios, in particular so for a heavy incident ion. Conversely, the flux at the surface is to some degree collimated around the direction of specular reflection, most pronouncedly so for light incident ions.

The leftmost flux diagram in the middle row of figure 8 may be compared with a graph computed by ROSENDAAL ET AL. (1982) for $m = 1/3$ and equal masses

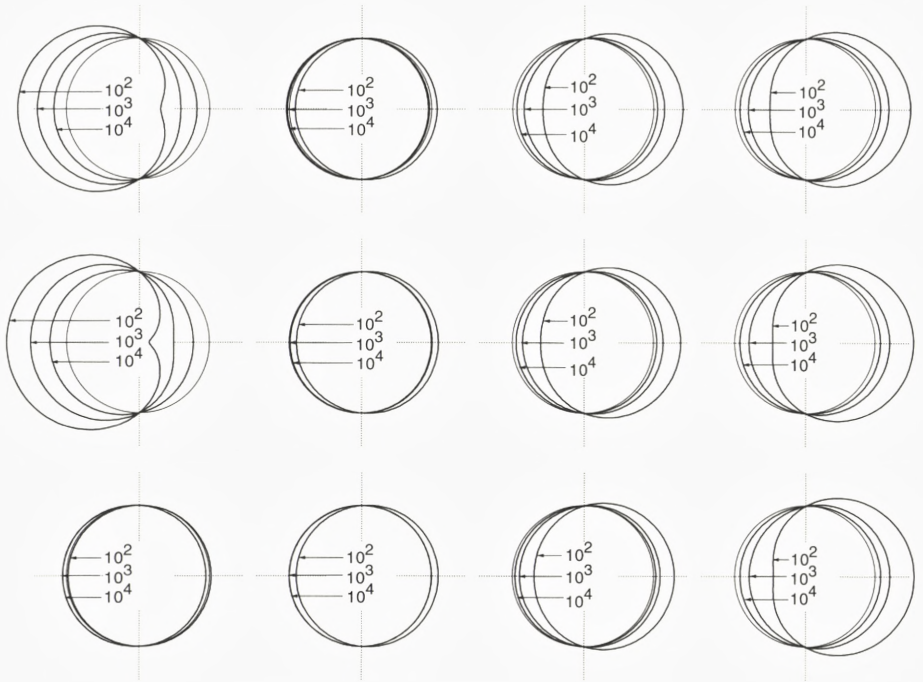


Figure 9: Same as figure 8 for $m = 0.2$

where a dramatic discrepancy is found. We note first that a relation for the flux equivalent with eq. (39) on page 23 was not derived in that work. Instead, an expression for the freezing density mentioned in section 2.2 (page 7) was adopted and written as a sum of two terms proportional to the density of deposited energy and momentum, respectively. The qualitative behavior for $E/W \gtrsim 10^2$ is similar to our finding although we find the anisotropy noticeably more pronounced at $E/W \simeq 100$. A major part of the diagrams given by ROSENDAAL ET AL. exhibit an inward anisotropy. This feature is related directly to regions of positive momentum deposition in the negative halfspace for $E/W \simeq 10$ or less, an unphysical behavior which we have asserted above to indicate the limits of the asymptotic expansion in powers of E/W .

7.6 General Behavior of the Anisotropy Factor

If only the first term in the brackets of eq. (39) on page 23 is kept one obtains a widely used expression for the flux density in an atomic collision cascade. This

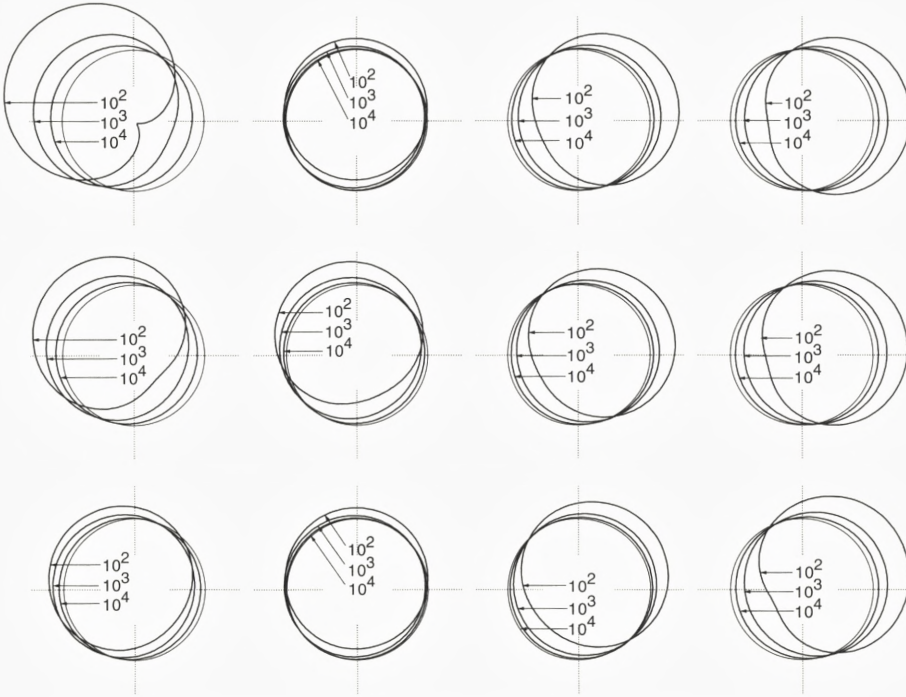


Figure 10: Same as figure 8 for angle of incidence 45° (from 'southwest').

expression represents an isotropic velocity distribution of recoil atoms and has been the starting point for estimates of sputtered-particle fluxes in the traditional backward and the less common transmission geometry (SIGMUND, 1981). Here we are interested in the limitations of and corrections to this expression. Deviations may be expressed by way of an anisotropy parameter $\mathcal{P}(x)$ defined as

$$\mathcal{P}(x) = \frac{G(E, \mathbf{e}; W, \boldsymbol{\Omega}, x)}{G_{\text{iso}}(E, \mathbf{e}; W, \boldsymbol{\Omega}, x)} = 1 - K_m(\boldsymbol{\Omega} \cdot \mathbf{e}_x) \frac{W}{NS(W)} \frac{\partial F_D(E, \mathbf{e}; x) / \partial x}{F_D(E, \mathbf{e}; x)} + 3 \frac{W}{\sqrt{2MW}} \frac{\boldsymbol{\Omega} \cdot \mathbf{F}_P^0(E, \mathbf{e}; x)}{F_D(E, \mathbf{e}; x)}, \quad (62)$$

where G_{iso} represents the zero-order (isotropic) approximation to eq. (39). A factor of this type was discussed by ROSENDAAL ET AL. (1982), based, however, on an expression for the freezing density instead of the particle flux. Moreover, the expression utilized did not contain a gradient term explicitly. We have plotted contour lines of $\mathcal{P}(x)$ in figures 8 - 10 for the specific case of power scattering. The power approximation must be expected to break down in the limit of $W \ll E$

which is of greatest interest in practice. We shall in this paragraph try to estimate the behavior of $\mathcal{P}(x)$ more broadly.

It has been argued in section 4.4 (page 19) that a more comprehensive description may be based on two power cross sections, one applying to the range near the initial energy, $\lesssim E$ and the other to the range near the instantaneous energy, $\gtrsim W$. This feature has already been incorporated into the notation employed in eq. (62) where the only explicit occurrence of a power exponent lies in the numerical constant K_m . The arguments put forward in sections 4.4 and 5.5 strongly suggest that m in K_m be chosen in accordance with the scattering law at energies $\gtrsim W$. For $W \ll E$ this typically implies that $m < 0.25$, i.e., K_m (figure 1) becomes positive in accordance with its significance as a diffusion term.

Consider first the last term in eq. (62) and note that

$$\begin{aligned} \frac{W}{\sqrt{2MW}} &\propto W^{1/2} \\ \frac{\boldsymbol{\Omega} \cdot \mathbf{F}_P^0(E, \mathbf{e}; x)}{F_D(E, \mathbf{e}; x)} &\propto E^{-1/2}. \end{aligned}$$

The energy dependence of this contribution to $\mathcal{P}(x)$ is given by $\sqrt{W/E}$. While the high-energy scattering law enters through the ratio of \mathbf{F}_P^0/F_D there is no explicit or implicit dependence on the low-energy scattering law. Hence, this contribution will be negligible for, say $W/E \ll 0.01$.

The behavior of the second term in eq. (62) is quite different. Here we have

$$\begin{aligned} \frac{W}{NS(W)} &\propto \frac{W^{2m}}{NC} \\ \frac{\partial F_D(E, \mathbf{e}; x)/\partial x}{F_D(E, \mathbf{e}; x)} &\propto \frac{NC_0}{E^{2m_0}}, \end{aligned}$$

where C_0 is a constant defining a power cross section according to eq. (25) (page 15) along with m_0 . This contribution is governed by $R(W)/R_0(E)$, where R and R_0 stand for slowing-down ranges of recoil and projectile, respectively. Since the nuclear stopping power decreases at low energy, ranges approach zero more slowly than what would be expected from the high-energy behavior (LINDHARD ET AL., 1963b). Therefore the anisotropy correction from the gradient term approaches zero more slowly than that of the momentum term. Consequently, deviations of the anisotropy parameter from unity for $W/E \ll 0.01$ are governed mainly by the gradient term.

For a more quantitative statement we need an estimate of F_D . Since only the logarithmic derivative enters into $\mathcal{P}(x)$ that estimate does not need to be very precise. We therefore approximate the deposited-energy profile by the Edgeworth

approximation which, in the leading term, assumes a gaussian profile for given mean depth $\langle x \rangle_D$ and width $\langle \Delta x^2 \rangle_D$. In the notation of SIGMUND (1968) we find

$$F_D(x) \sim \frac{E}{\sqrt{\langle \Delta x^2 \rangle_D}} \Phi_0(\xi) \left(1 + \frac{1}{6} \Gamma_1 \text{He}_3(\xi) \dots \right),$$

where $\Phi_0(\xi) = \exp(-\xi^2/2)/\sqrt{2\pi}$ and $\text{He}_n(\xi)$ are Hermite polynomials in the notation of ABRAMOWITZ & STEGUN (1964). Moreover,

$$\xi = \frac{x - \langle x \rangle_D}{\sqrt{\langle \Delta x^2 \rangle_D}}; \quad \Gamma_1 = \frac{\langle \Delta x^3 \rangle_D}{\langle \Delta x^2 \rangle_D^{3/2}}$$

and hence,

$$\frac{\partial \log F_D}{\partial x} \sim \frac{1}{\sqrt{\langle \Delta x^2 \rangle_D}} \left(-\xi + \frac{\Gamma_1}{2} \text{He}_2(\xi) \dots \right).$$

This yields a rough estimate of the anisotropy factor,

$$\mathcal{P}(x) \simeq 1 - K_m(\mathbf{\Omega} \cdot \mathbf{e}_x) \frac{W}{NS(W)} \left(\frac{\langle x \rangle_D - x}{\langle \Delta x^2 \rangle_D} + \frac{\langle \Delta x^3 \rangle_D}{2\langle \Delta x^2 \rangle_D^2} \left[\frac{(x_D - x)^2}{\langle \Delta x^2 \rangle_D} - 1 \right] \dots \right)$$

For the qualitative behavior we consider only the first term in the parentheses, corresponding to a gaussian profile. It is seen that the deviation from $\mathcal{P}(x) = 1$ is directed inward for $x > \langle x \rangle_D$ and outward for $x < \langle x \rangle_D$. In particular, for $x = 0$ it goes as E^{-2m} , i.e., the sputtered flux becomes *increasingly overcosine* with decreasing incident energy.

7.7 Power-Law Anisotropy

It has become customary to characterize the angular dependence of an anisotropic particle flux by a power law of the form

$$f(\cos \theta) \simeq A |\cos^n \theta| \tag{63}$$

with constants n and A . In the present picture, particle fluxes come out in the form of

$$g(\cos \theta) \simeq B |\cos \theta| (1 + b |\cos \theta|)$$

with constants b and B . For overcosine distributions we have $n > 1$ and $b > 0$. In the opposite case distributions are under cosine.

We may express one description by the other by choosing constants A, B such that f and g are normalized to the same value (e.g. 1) and by equating the values

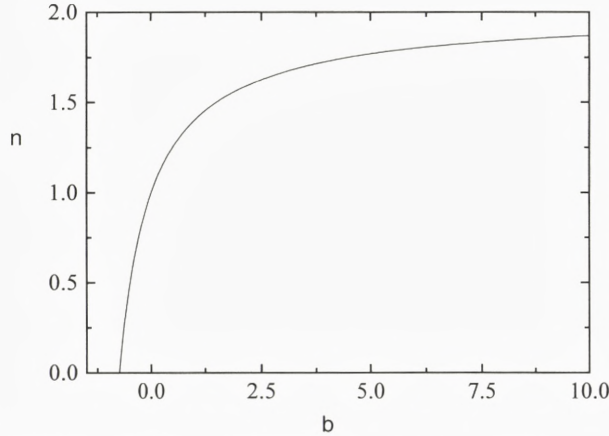


Figure 11: Matching angular anisotropy to a power-law profile, eq. (63) by means of eq. (64)

of the two functions at normal emergence $\theta = 0$. This requirement, which could also be used to extract n from measurements, yields

$$n = 1 + \frac{2b}{3 + 2b}. \quad (64)$$

The resulting relationship is illustrated in figure 11.

8 Discussion

8.1 Deposited Momentum and Energy

It was established long ago (WINTERBON ET AL., 1970) that the spatial distribution of deposited energy is a well-defined quantity in both one and three dimensions to the extent that a limiting value exists when the freezing energy U approaches zero.

The behavior of the deposited-momentum profile is more complicated. In early work (LITTMARK, 1974; LITTMARK & SIGMUND, 1975), a vector distribution was evaluated which had scaling properties with the beam energy similar to those of the deposited energy and had the right normalization. This function, which is identical with \mathbf{F}_P^0 in eq. (39) on page 23, has weaknesses that were recognized early on but removed only gradually.

The fact that this profile showed a physically acceptable behavior only for $m > 0.25$ was recognized immediately (SANDERS, 1968). The fact that the momentum

profile must be sensitive to the freezing energy U can be extracted from the work of ROOSEENDAAL ET AL. (1982) who, implicitly, included terms going beyond F_P^0 in their analysis. The existence of a gradient term, normalized to zero and having scaling properties in angle and energy different from F_P^0 was established only very recently (SCKERL ET AL., 1995; GLAZOV, 1995). The present work adds little new to this, except for the fact that our momentum profiles, evaluated numerically by the Padé method, agree well with those of ROOSEENDAAL ET AL. (1982) where comparison is possible, and that there are minor differences from those of GLAZOV (1995) in the limit of low freezing energies.

The most important lesson to be learned from these studies is the fact that unlike measurements of energy, measurements of momentum are sensitive to threshold effects including binding energies. This may be illustrated on sputtering data. It was predicted theoretically (SIGMUND, 1968) and confirmed experimentally (ANDERSEN, 1970, 1971) that the main material parameters determining the energy reflection coefficient (or sputter efficiency), are the mass and atomic number while the cohesive energy is insignificant. An attempt (SIGMUND, 1968) to extract a similar behavior from measurements of the reflected momentum (KOPITZKI & STIER, 1961, 1962) failed. One likely reason for this must be the lack of simple scaling properties. Therefore, studying deposited momentum as a goal in itself is not necessarily attractive.

With regard to the results presented in figures 3 - 7 (pp. 38-42) we recall that the assumption of $E \gg U$ is essential, and that deviations from asymptotic behavior show up for $E/U \lesssim 10$. The occurrence of a positive momentum profile at negative depths ($x < 0$) is indicative of a breakdown of the asymptotic picture. This was apparently not noticed by ROOSEENDAAL ET AL. (1982). Implications from this behavior which entered the literature subsequently (HAUTALA & WHITLOW, 1985) need to be taken with caution.

8.2 Particle Flux in Bulk

Several attempts have been made to estimate anisotropic particle fluxes as well as energy and momentum fluxes in the literature. In this paragraph we consider bulk fluxes where complications due to surface discontinuities are of no or only minor importance. Effects of regular crystal structure are ignored.

Not all estimates address flux densities G or fluxes $G|\cos\theta|$ as defined in the present paper. LITTMARK & HOFER (1980), in addressing recoil mixing, evaluated recoil densities, and ROOSEENDAAL ET AL. (1982) estimated freezing densities. However, within the approach chosen in those papers there should be no major differences between the anisotropy factors belonging to various distributions. This, however, ignores the existence of the gradient term which was not recognized until

recently (SCKERL ET AL., 1995). According to section 7.6 this term dominates over the momentum term in the limit of $E \gg W$. Conversely, the estimates mentioned above appear significant for moderate ratios of E/W . Such ratios are relevant in the theory of collisional mixing, the topic addressed by LITTMARK & HOFER (1980).

HAUTALA & WHITLOW (1985) evaluated fluxes of particles and momentum for argon bombardment of germanium by Monte Carlo simulation. The results are qualitative because of moderate statistics. Moreover, fluxes were recorded at five distinct depths which were kept fixed even when the incident energy was varied from 10 to 80 keV. Nevertheless, several features emerging from the present work are consistent with their findings. The graph in the upper left corner of figure 8 may be employed as a rough illustration of 80 keV Ar ions incident on Ge. In agreement with the simulations we find a very low forward flux at the surface but a rapid change toward isotropy with increasing depth. This qualitative feature does not change dramatically with energy but a comparison between figures 8 and 9 indicates a certain sensitivity to the interaction potential, a feature that emerged already from the simulations.

While the angular distributions shown in figures 8 - 10 (pp. 43-45) refer to fluxes differential in energy, the fluxes found in the simulations of HAUTALA & WHITLOW (1985) are integrated over all energies. However, a second integral is given where the particle flux has been weighted by momentum and hence reflects a higher contribution of high-energy recoil atoms. In the language of figures 8 - 10 this is equivalent with a lower value of E/W and, hence, a higher degree of anisotropy. Also here we find good qualitative agreement between simulation and transport theory.

8.3 Collisional Mixing

Our findings have implications on the theory of collisional mixing. It is common to distinguish between recoil implantation, i.e., relocation of atoms knocked on by primary ions, and cascade mixing dealing with the effect of higher-generation recoils (LITTMARK & HOFER, 1980; SIGMUND & GRAS-MARTI, 1981). Here we deal with cascade mixing which is conventionally based upon the recoil density, i.e., a distribution in energy, angle, and depth of recoiling atoms in combination with a range-energy relation for recoils. The recoil density is closely related to the particle flux. Elementary theory of cascade mixing is based on the asymptotic limit of an isotropic velocity distribution. A term corresponding to the \mathcal{B} -family is taken into account routinely in some codes, following the scheme outlined by LITTMARK & HOFER (1980). No allowance has hitherto been made for inclusion of a gradient term following from the \mathcal{C} -family.

The recoil density can easily be expressed by the flux density on the basis of the definition,

$$F(E, e; W, \Omega, x) = N \int dW' \int d^2\Omega' G(E, e; W', \Omega', x) K(W', \Omega'; W, \Omega).$$

The resulting expression for the recoil density is found from eq. (39) on page 23 by integration of the first term according to

$$\int_{W' > W} dW' K(W', W)$$

and the two subsequent terms according to

$$\int_{W' > W} dW' K(W', W) \sqrt{W/W'}.$$

In practice, these expressions would have to be written up for multicomponent media in accordance with the scheme outlined in appendix A.

From this we readily find the conventional W^{-2} term in the recoil density (SIGMUND, 1969a; 1972) as well as correction terms $\propto W^{2m-2}$ and $\propto W^{-3/2}$ for the \mathcal{C} and \mathcal{B} family, respectively. The existence of the latter has been recognized in principle long ago (SANDERS, 1968) and was utilized with the correct coefficients by LITTMARK & HOFER (1980). The gradient term $\propto W^{2m-2}$ is new. It is seen that for low-energy recoils, where m is small, the dependence on recoil energy W is very similar to that of the leading \mathcal{A} term. In ion beam mixing, mostly the projected relocation depth is of interest. The most pronounced modification to the isotropic approximation is, therefore, a forward-backward asymmetry which may be estimated from figures 8 - 10 on the basis of the following relationship,

$$\begin{aligned} \mathcal{P}_{\text{flux}} &= \mathcal{P} = 1 + \delta\mathcal{P}_B + \delta\mathcal{P}_C \\ \mathcal{P}_{\text{recoil}} &= 1 + \delta\mathcal{P}_B + \frac{2}{3} \frac{1-m}{1-2m} \delta\mathcal{P}_C, \end{aligned}$$

where $\delta\mathcal{P}_B$ and $\delta\mathcal{P}_C$ are defined by eq. (62). It is seen that for $m = 0$ the anisotropy in the recoil density is smaller by 33 % than that in the flux due to a smaller \mathcal{C} correction, while for $m = 0.25$ the two anisotropy factors are identical. Therefore, as a first approximation, figures 8 - 10 may be taken also as estimates of the anisotropy factor of the recoil density. Evidently, mixing profiles will be asymmetric, and the transition from profiles skewing outward to profiles skewing inward lies around $\langle x \rangle_D - \Delta x_D$.

8.4 Particle Flux at Surface

The backward particle flux at a bombarded surface is measured by sputtering experiments. In addition to measurements of the absolute sputter yield, dependent

on ion energy and angle of incidence, measurements of the distribution in ejection angle and/or energy are of interest in the present context. For quantitative comparisons with experiment it is necessary to account for surface binding. This is conventionally achieved by imposing a planar or, occasionally, spherical surface barrier. A correction for multiple crossings of the surface in an infinite medium is necessary in principle but has only rarely been performed in practice, but an exact evaluation for a solvable model has been performed by URBASSEK & VICANEK (1988).

8.5 Sputter Yield

Disregarding the surface correction and adopting a planar potential barrier U_s so that $W \geq U_s/\cos^2\theta$, we find the following expression for the sputter yield,

$$Y(E, \mathbf{e}) = \frac{\Gamma_m U_s^{2m}}{2 NC} \left[\frac{1}{4(1-2m)} \frac{F_D(E, \mathbf{e}; 0)}{U_s} + K_m \frac{1-m}{(1-4m)(5-8m)} \frac{\partial F_D(E, \mathbf{e}; x)/\partial x|_{x=0}}{NS(U_s)} - \frac{3}{2(1-4m)} \frac{F_{P,x}^0(E, \mathbf{e}; 0)}{\sqrt{2MU_s}} \right], \quad (65)$$

where the first term is identical with the one derived long ago (SIGMUND, 1969b). The correction terms are new in this form, but the third one, which is less important than the second, has been invoked more or less explicitly in previous treatments (e.g., MATSUNAMI ET AL., 1984). We note that a frequently quoted estimate of that term (ROOSENDAAL & SANDERS, 1980) had the wrong sign since it was based on the deposited momentum integrated over all space which is directed inward.

For $m \ll 1$ we may ignore the last term in the brackets of eq. (65). The gradient term constitutes a positive correction to the asymptotic sputter yield which increases toward lower beam energies. This is one likely reason for the good agreement between measured sputter yields and the asymptotic sputter yield formula (SIGMUND, 1969b) when evaluated with the Thomas-Fermi stopping cross section which is known to fall off too slowly with decreasing beam energy. Since $S(U_s) \propto U_s^{1-2m}$, the dependence of the yield on U_s is hardly affected.

On the theoretical side, eq. (65) appears to accentuate the need for a proper surface correction since $\partial F_D/\partial x$ varies more rapidly near $x = 0$ than F_D .

8.6 Differential Sputter Fluxes

The effect of the gradient term in the sputter flux will be visible in the distribution in emission angle. The energy spectrum, on the other hand, is rather insensitive for small values of m .

Angular dependencies are characterized experimentally by an exponent n as defined by eq. (63) which may be related to the anisotropy factor \mathcal{P} by eq. (64) with

$$b = K_m \frac{W}{NS(W)} \left. \frac{\partial F_D / \partial x}{F_D} \right|_{x=0}. \quad (66)$$

We note that this relation determines the flux at an emission energy W which has not been corrected for a planar surface barrier. Measured angular distributions refer typically to the flux integrated over all emission energies. Nevertheless we may extract a dependence of n on the ion energy E from eqs. (64) and (66). Since $b \propto E^{-2m_0}$ we may conclude that n approaches 1 at high beam energies as $1 + \text{const} \times E^{-2m_0}$, while it varies more slowly at lower beam energies. The maximum possible value of n in this description is $n = 2$ which, according to eq. (64), is reached for $2b \gg 3$, i.e., for highly anisotropic flux distributions for which several of our approximations would break down. However, these results are modified in the presence of a real surface (WALDEER & URBASSEK, 1987, 1988; URBASSEK & VICANEK, 1988).

Measurements (ANDERSEN ET AL., 1985) as well as Monte Carlo simulations (HAUTALA & WHITLOW, 1985) on Ar-Ge indicate a maximum value of $n \simeq 1.6$ and 1.7, respectively, in the medium-keV range (~ 20 keV for the experimental data), i.e., $b \sim 2$. This is certainly too large an anisotropy to be counted as a weak perturbation. Thus, while the decrease in n above the maximum may be accounted for, the behavior at lower energies is outside the range of validity of our description.

8.7 Isotope Effect

For an extensive review of the isotope effect in sputtering the reader is referred to SIGMUND & LAM (1993). It was suggested some time ago that nonstoichiometric particle fluxes found in computer simulations of cascades in isotopic mixtures were related to momentum balance (SHAPIRO ET AL., 1988). Isotope effects in the particle flux were studied long ago (ANDERSEN & SIGMUND, 1974), and a slight dominance of the light isotope(s) was derived for the isotropic part, cf. eq. (58).

A more recent study by two of us addressing the \mathcal{B} -term (SIGMUND & SCKERL, 1993) revealed two isotope dependencies, one identical with the one inherent in the \mathcal{A} -term and an additional one preferring the heavier species, cf. eq. (59). The combined effect in the \mathcal{B} -contribution to the particle flux typically prefers the heavier species, but in view of the smallness of that contribution in comparison with the isotropic particle flux, this effect was considered to be rather insignificant.

Since the gradient term is at least as important a correction to the isotropic particle flux, the sign and magnitude of its isotope dependence is relevant in this

context. Eq. (60) in conjunction with figure 2 indicates the \mathcal{C} -term to be preferential in the heavy isotope(s). For $m < 0.25$, that preference is, however, less pronounced than in the \mathcal{B} -term. This implies that the conclusions drawn by two of us (SIGMUND & SCKERL, 1993) on the significance of momentum asymmetry in isotope sputtering are essentially unaffected by the gradient contribution which was not known to us at the time.

A recent study of isotope sputtering by numerical simulation (SHULGA & SIGMUND, 1995, 1996) has shown that at high ion energies, nonstoichiometric particle fluxes obey essentially eq. (58) as one would expect. Very pronouncedly nonstoichiometric sputter fluxes are found at low energies which involve primary recoil atoms and threshold processes. These effects are so pronounced that even though they decrease in importance with increasing energy, they appear to overshadow the \mathcal{B} - and \mathcal{C} -contributions to the particle flux at least in the case studied (Ar on Mo).

Appendix

A Polyatomic Materials

This section lists generalizations of some of the basic equations as well as results of the present work to polyatomic media. Unless stated otherwise definitions and proofs follow the same line as indicated in the main text so that the main complication lies in notation.

A.1 Fundamentals

The relations (3) defining deposited energy and momentum expand to

$$\begin{aligned} F_{D,j}(\mathbf{r}, U) &= \int_{W < U} d^3\mathbf{w} W F_j(\mathbf{w}, \mathbf{r}, U), \\ \mathbf{F}_{P,j}(\mathbf{r}, U) &= \int_{W < U} d^3\mathbf{w} M_j \mathbf{w} F_j(\mathbf{w}, \mathbf{r}, U) \end{aligned}$$

where the freezing density $F_j(\mathbf{w}, \mathbf{r}, U)$ now refers to atoms of species j . Mainly accumulated densities of energy and momentum

$$\begin{aligned} F_D(\mathbf{r}, U) &= \sum_j F_{D,j}(\mathbf{r}, U) \\ \mathbf{F}_P(\mathbf{r}, U) &= \sum_j \mathbf{F}_{P,j}(\mathbf{r}, U) \end{aligned}$$

deposited in all species are of interest, except for the considerations presented in appendix B³⁴.

The fundamental relation (4) expressing the freezing density by the flux densities reads

$$F_j(\mathbf{w}, \mathbf{r}, U) = \sum_k \sum_l N_l(\mathbf{r}) \int_{W' > U} d^3 \mathbf{w}' G_k(\mathbf{w}', \mathbf{r}) \int d\sigma_{kl}(\mathbf{w}'; \mathbf{v}', \mathbf{v}'') \\ \times \left(\delta_{kj} \delta(\mathbf{v}' - \mathbf{w}) + \delta_{lj} \delta(\mathbf{v}'' - \mathbf{w}) \right), \quad (W < U).$$

With this the relations (8) between deposited energy and momentum and the flux densities are generalized to

$$F_D = \sum_{j,k} \int_{W > U} dW \left(G_j(W) N_k \int_{E' < U} E' d\sigma_{jk} + G_k(W) N_j \int_{E'' < U} E'' d\sigma_{kj} \right) \\ F_P = \sum_{j,k} \int_{W > U} dW \left(\mathbf{H}_j(W) N_k \int_{E' < U} M_j v' \cos \phi' d\sigma_{jk} \right. \\ \left. + \mathbf{H}_k(W) N_j \int_{E'' < U} M_j v'' \cos \phi'' d\sigma_{kj} \right)$$

where

$$G_j(W) = \int d^2 \Omega G_j(W, \Omega) \\ \mathbf{H}_j(W) = \int d^2 \Omega \Omega G_j(W, \Omega).$$

From elastic-collision dynamics we obtain a generalization of eq. (10) for the longitudinal momentum component transferred from a j -atom with energy W hitting a k -atom at rest,

$$M_j v' \cos \phi' = \frac{2}{w} (W - \beta_{jk} T)$$

where

$$\beta_{jk} = \frac{M_j + M_k}{2M_j}.$$

³Subscripts j and i are applied here to avoid mixing up energy/momentum deposited in j atoms, $F_{D,j}(\mathbf{r}, U)$, $\mathbf{F}_{P,j}(\mathbf{r}, U)$, with energy/momentum deposited due to bombardment with i -atoms to be introduced below.

⁴A species-dependent threshold U_j could in principle be introduced but has no function within the context of the present work.

Similarly, for a k -atom with energy W hitting a j -atom at rest we have

$$M_j v'' \cos \phi'' = \frac{2}{w} \beta_{kj} T.$$

This yields

$$F_D = \sum_{j,k} \int_{W>U} dW \left(G_j(W) N_k S'_{jk}(W, U, 1) + G_k(W) N_j S''_{kj}(W, U, 1) \right)$$

$$F_P = \sum_{j,k} \int_{W>U} dW \frac{2}{w} \left(\mathbf{H}_j(W) N_k S'_{jk}(W, U, \beta_{jk}) + \mathbf{H}_k(W) N_j S''_{kj}(W, U, \beta_{kj}) \right)$$

where

$$S'_{jk}(W, U, \beta_{jk}) = \int_{T>W-U} (W - \beta_{jk} T) d\sigma_{jk}(W, T)$$

$$S''_{kj}(W, U, \beta_{kj}) = \beta_{kj} \int_{T<U} T d\sigma_{kj}(W, T)$$

instead of eqs. (11-13).

A.2 Transport Equations

The transport equations for polyatomic media were established already in Boltzmann's original work (BOLTZMANN, 1875). The linearized versions are listed here only for definiteness of notation. The forward equation (17) reads

$$\sum_k \int d^3 \mathbf{w}' \int d^3 \mathbf{w}'' \left\{ G_j(\mathbf{w}) K_{jk}(\mathbf{w}; \mathbf{w}', \mathbf{w}'') N_k - G_j(\mathbf{w}') K_{jk}(\mathbf{w}'; \mathbf{w}, \mathbf{w}'') N_k \right. \\ \left. - G_k(\mathbf{w}') K_{kj}(\mathbf{w}'; \mathbf{w}'', \mathbf{w}) N_j \right\} + \cos \theta \frac{\partial}{\partial x} G_j(\mathbf{w}) = \delta_{ij} \delta(\mathbf{w} - \mathbf{v}) \delta(x),$$

while the backward equation (18) turns into

$$\sum_k N_k \int d\sigma_{ik}(\mathbf{v}; \mathbf{v}', \mathbf{v}'') \left\{ G_{ij}(\mathbf{v}) - G_{ij}(\mathbf{v}') - G_{kj}(\mathbf{v}'') \right\}, \\ + \cos \Theta \frac{\partial}{\partial x} G_{ij}(\mathbf{v}) = \delta_{ij} \delta(\mathbf{v} - \mathbf{w}) \delta(x). \quad (67)$$

The normalization relations (21) and (22) remain valid also for deposited energy $F_{D,i}$ and momentum $F_{P,i}$ while the transport equation reads

$$\sum_k N_k \int \left\{ F_{D,i}(\mathbf{v}) - F_{D,i}(\mathbf{v}') - F_{D,k}(\mathbf{v}'') \right\} d\sigma_{ik}(\mathbf{v}; \mathbf{v}', \mathbf{v}'') \\ + \cos \Theta \frac{\partial}{\partial x} F_{D,i}(\mathbf{v}) = 0.$$

Here, $F_{D,i}$ indicates the energy deposited in all species due to bombardment with an i -particle. The equation for F_P is expanded analogously.

A.3 Solutions

The flux equations eq. (67) may be transformed into Laplace space and thus form a generalized version of eq. (26). The resulting multidimensional system of algebraic equations splits into uncoupled sets of equations, one for each target species j and, for $n = 0$, one for each combination of $\ell = \ell'$ and $\mu = \mu'$. Solutions may then be found in accordance with the scheme outlined long ago (ANDERSEN & SIGMUND, 1974). Pertinent terms were selected on the basis of the criteria developed in conjunction with tables I and II above. Explicit results quoted here refer to a binary medium with arbitrary masses M_1, M_2 and elastic scattering. The leading moments in the three families then read

$$G_{i1}^{A(0)} = \frac{E}{4\pi W^2} \frac{N_1 S_{21}(W)}{W D'_A(1)} \quad (68)$$

$$G_{i1}^{B(0)} = \frac{3(\mathbf{e} \cdot \boldsymbol{\Omega})}{4\pi W} \sqrt{\frac{2M_i E}{2M_1 W}} \frac{M_1 + M_2}{2M_2} \frac{N_1 S_{21}(W)}{W D'_B(1/2)} \quad (69)$$

$$G_{i1}^{C(1)} = \frac{3(\mathbf{e}_x \cdot \boldsymbol{\Omega})E}{W^2 D'_A(1)} \left(N_1 S_{21}(W) \overline{G}_{11;10;10}^{(0)}(1 - 2m) \right. \\ \left. + N_2 S_{12}(W) \overline{G}_{21;10;10}^{(0)}(1 - 2m) \right) \quad (70)$$

where $D_A(s), D_B(s)$ are determinants that have been discussed previously (ANDERSEN & SIGMUND, 1974; SIGMUND & SCKERL, 1994) which in the present notation read

$$D(s) = \left(\Sigma'_{11,\ell} - \Sigma''_{11,\ell} + \Sigma'_{12,\ell} \right) \left(\Sigma'_{21,\ell} + \Sigma'_{22,\ell} - \Sigma''_{22,\ell} \right) - \Sigma''_{12,\ell} \Sigma''_{21,\ell}$$

with $\ell = 0, 1$ for D_A, D_B , respectively, expressed in terms of macroscopic transport cross sections

$$\Sigma'_{ik,\ell}(s) = N_k \int d\sigma_{ik} \left\{ 1 - P_\ell(\cos \phi') (1 - t)^s \right\} \quad (71)$$

$$\Sigma''_{ik,\ell}(s) = N_k \int d\sigma_{ik} P_\ell(\cos \phi'') t^s. \quad (72)$$

Primes in the determinants indicate derivatives with respect to s .

The Laplace moments can be written in the form

$$\overline{G}_{11;10;10}^{(0)}(s) = \frac{\Sigma'_{21,1}(s) + \Sigma'_{22,1}(s) - \Sigma''_{22,1}(s)}{12\pi W D_B(s)}$$

$$\overline{G}_{21;10;10}^{(0)}(s) = \frac{\Sigma''_{21,1}(s)}{12\pi W D_B(s)}.$$

From this we reconstruct the spatial distribution of the flux density of 1-atoms according to

$$G_{i1}(E, \mathbf{e}; W, \boldsymbol{\Omega}, x) = G_{i1}^A + G_{i1}^B + G_{i1}^C$$

with

$$G_{i1}^A = \frac{F_{D,i}(E, \mathbf{e}; x)}{4\pi W^2} \frac{N_1 S_{21}(W)}{W D'_A(1)} \quad (73)$$

$$G_{i1}^B = \frac{3}{4\pi W} \frac{\boldsymbol{\Omega} \cdot \mathbf{F}_{P,i}^0(E, \mathbf{e}; W, \boldsymbol{\Omega}, x)}{\sqrt{2M_1 W}} \left(\frac{M_1 + M_2}{2M_2} \right) \frac{N_1 S_{21}(W)}{W D'_B(1/2)} \quad (74)$$

$$G_{i1}^C = -\frac{3(\mathbf{e}_x \cdot \boldsymbol{\Omega})}{W^2 D'_A(1)} \frac{\partial F_{D,i}(E, \mathbf{e}; W, \boldsymbol{\Omega}, x)}{\partial x} \\ \times \left(N_1 S_{21}(W) \overline{G}_{11;10;10}^{(0)}(1 - 2m) + N_2 S_{12}(W) \overline{G}_{21;10;10}^{(0)}(1 - 2m) \right) \quad (75)$$

where $F_{D,i}(E, \mathbf{e}; x)$ is the density of deposited energy for bombardment with an i -particle and $\mathbf{F}_{P,i}^0(E, \mathbf{e}; W, \boldsymbol{\Omega}, x)$ the corresponding momentum density.

The corresponding flux density of 2-atoms is found by interchanging indices. These results have been utilized in the evaluations reported in section 6.6.

B Conservation Laws

This section serves primarily to clarify the physical significance of some of the statistical distribution functions introduced in section 2.3 and their generalizations to polyatomic media in appendix A. Well-known results on energy sharing are shown to emerge directly from conservation laws of energy and momentum in considerable generality.

B.1 Energy Conservation

Consider first elastic collisions in a monoatomic medium. Differentiation of eq. (11) with respect to U yields

$$\frac{\partial F_D}{\partial U} = NU \int dW \left\{ G(W)K(W, W - U) + G(W)K(W, U) - G(U)K(U, W) \right\},$$

where $K(E, T) = d\sigma(E, T)/dT$. On the other hand, integration over $\boldsymbol{\Omega}$ of the forward equation (15) leads to

$$N \int dW' \left\{ G(W)K(W, W') - G(W')K(W', W' - W) \right. \\ \left. - G(W')K(W', W) \right\} + \nabla \cdot \mathbf{H}(W) = \delta(W - E)\delta(\mathbf{r}).$$

After elimination of the integral we find

$$-\frac{\partial F_D}{\partial U} + \nabla \cdot (U \mathbf{H}(U)) = E \delta(U - E) \delta(\mathbf{r})$$

which has the form of a continuity equation expressing energy conservation. Before discussing its significance we note first that for a polyatomic medium this relation expands to

$$-\frac{\partial F_{D,j}}{\partial U} + \nabla \cdot (U \mathbf{H}_j(U)) + \sum_k \left\{ G_j(U) N_k S_{jk}(U) - G_k(U) N_j S_{kj}(U) \right\} = \delta_{ij} E \delta(U - E) \delta(\mathbf{r}).$$

We may also allow for electronic stopping by formally considering target electrons as being one of the species entering the k -sum. Disregarding energy transfer from electrons to nuclei and expressing the electronic stopping power by stopping cross sections of individual atoms (Bragg's rule) we arrive at

$$-\frac{\partial F_{D,j}}{\partial U} + \nabla \cdot (U \mathbf{H}_j(U)) + \sum_k \left\{ G_j(U) N_k S_{jk}(U) - G_k(U) N_j S_{n,kj}(U) \right\} = \delta_{ij} E \delta(U - E) \delta(\mathbf{r}), \quad (76)$$

where

$$S_{jk}(U) = S_{n,jk}(U) + S_{e,jk}(U)$$

and $S_{n,jk}(U)$, $S_{e,jk}(U)$ denote the nuclear and electronic stopping cross section, respectively, of a j -atom colliding with a k -atom.

The physical significance becomes most illuminating after integration over some arbitrary ΔV as well as some energy interval $U_1 < U < U_2 < E$, and use of Gauss' theorem,

$$\begin{aligned} \mathcal{E}_j(\Delta V, U_1) - \mathcal{E}_j(\Delta V, U_2) = & \int_{U_1}^{U_2} dU \left\{ - \int_{S(\Delta V)} d^2 \mathbf{r} \mathbf{n} \cdot (U \mathbf{H}_j(U, \mathbf{r})) \right. \\ & \left. + \int_{\Delta V} d^3 \mathbf{r} \sum_k \left(-G_j(U, \mathbf{r}) N_k S_{jk}(U) + G_k(U, \mathbf{r}) N_j S_{n,kj}(U) \right) \right\}, \end{aligned}$$

where

$$\mathcal{E}_j(\Delta V, U) = \int_{\Delta V} d^3 \mathbf{r} F_{D,j}(\mathbf{r}, U)$$

is the energy deposited per cascade in ΔV if the freezing energy is U , $S(\Delta V)$ is a closed surface surrounding ΔV and \mathbf{n} a unit vector in the direction of the outward surface normal.

We note first that

$$-dU \int_{S(\Delta V)} d^2r \left(U \mathbf{n} \cdot \mathbf{H}_j(U, \mathbf{r}) \right) = -dU \int_{S(\Delta V)} d^2r \int_0^\infty dt \int d^2\Omega (\mathbf{n} \cdot \mathbf{u}) g_j(U, \Omega, \mathbf{r}, t)$$

is the net flux of energy per cascade carried by j -atoms out of ΔV with energies in the interval (U, dU) . Here, \mathbf{u} denotes the velocity of a particle with energy U and direction Ω .

Next, the term

$$-dU \int_{\Delta V} d^3\mathbf{r} G_j(U, \mathbf{r}) \sum_k N_k S_{jk}(U)$$

accounts for all loss of energy from ΔV by nuclear and electronic collisions undergone by j -particles with energies (U, dU) , and

$$-dU \int_{\Delta V} d^3\mathbf{r} \sum_k G_k(U, \mathbf{r}) N_j S_{n,kj}(U)$$

accounts for the corresponding gain in the form of recoil atoms.

The net result of gains and losses is the energy of those j -atoms which freeze at energies in the interval (U_1, U_2) while in ΔV .

B.2 Momentum Conservation

A similar procedure may be applied to momentum. Differentiation of eq. (12) with respect to U yields

$$\frac{\partial \mathbf{F}_P}{\partial U} = NU \int dW \left\{ \frac{2}{w} \mathbf{H}(W) K(W, W - U) + \frac{2}{w} \mathbf{H}(W) K(W, U) - \frac{2}{u} \mathbf{H}(U) K(U, W) \right\}.$$

Now assume elastic collisions, multiply eq. (15) with Ω and integrate over Ω . This yields

$$N \int dW' \left\{ \mathbf{H}(W) K(W, W') - \mathbf{H}(W') \cos \phi' K(W', W' - W) - \mathbf{H}(W') \cos \phi'' K(W', W) \right\} + \nabla \cdot \mathbf{J}(W) = \mathbf{e} \delta(W - E) \delta(\mathbf{r}),$$

where $\cos \phi'' = w/w'$ and $\cos \phi' = w/w'$, and $\mathbf{J} = (J_{\alpha\beta})$ denotes a symmetric tensor with components

$$J_{\alpha\beta}(W) = \int d^2\Omega \Omega_\alpha \Omega_\beta G(W, \Omega), \quad \alpha, \beta = 1, 2, 3.$$

After elimination of the integral we find

$$-\frac{\partial \mathbf{F}_P}{\partial U} + \nabla \cdot \left(\sqrt{2MU} \mathbf{J}(U) \right) = M\mathbf{v}\delta(U - E)\delta(\mathbf{r}).$$

For a polyatomic medium this expands to

$$-\frac{\partial \mathbf{F}_{P,j}}{\partial U} + \nabla \cdot \left(\sqrt{2M_j U} \mathbf{J}_j(U) \right) + \sum_k \left\{ \mathbf{H}_j(U) N_k T_{jk}(U) - \mathbf{H}_k(U) N_j T_{kj}(U) \right\} = \delta_{ij} M_i \mathbf{v} \delta(U - E) \delta(\mathbf{r})$$

with the momentum transfer cross section

$$T_{jk}(W) = \int \sqrt{2M_k T} \cos \phi'' d\sigma_{jk}(W, T) = \frac{M_j + M_k}{\sqrt{2M_j W}} S_{jk}(W).$$

B.3 Applications

The above relations allow to rederive or confirm basic results for particle fluxes found in our previous work (ANDERSEN & SIGMUND, 1974; VICANEK ET AL., 1993; SIGMUND & SCKERL, 1993) by a unified procedure. First, consider spatial averages only where the divergence term disappears. Eq. (76) then reduces to the starting point of a study of energy spectra in multicomponent targets (VICANEK ET AL., 1993). If, furthermore, the U dependence of $F_{D,i}$ is disregarded — which should be justified for $U \ll E$ — we arrive at

$$\sum_k \left(G_j(W) N_k S_{jk}(W) - G_k(W) N_j S_{kj}(W) \right) = 0,$$

a relation first mentioned by ANDERSEN & SIGMUND (1974). For a binary medium, this reduces to

$$\frac{G_1(W)}{G_2(W)} = \frac{N_1 S_{21}(W)}{N_2 S_{12}(W)}.$$

Likewise, if the U dependence of $\mathbf{F}_{P,i}$ is insignificant one arrives at

$$\sum_k \left(\mathbf{H}_j(W) N_k T_{jk}(W) - \mathbf{H}_k(W) N_j T_{kj}(W) \right) = 0$$

which for a binary medium reduces to

$$\mathbf{H}_1 N_2 T_{12} = \mathbf{H}_2 N_1 T_{21},$$

a result found by two of us (SIGMUND & SCKERL, 1993).

Acknowledgements

We like to thank Lev Glazov and Herbert Urbassek for stimulating discussions and useful comments on the manuscript. This work was supported by the Danish Natural Science Research Council (SNF).

References

- M. Abramowitz and I. A. Stegun, 1964: *Handbook of Mathematical Functions*, Dover
- H. H. Andersen, 1970: *Radiat. Eff.* **3**, 51
- H. H. Andersen, 1971: *Radiat. Eff.* **7**, 179
- H. H. Andersen, B. Stenum, T. Sørensen, and H. J. Whitlow, 1985: *Nucl. Instrum. Methods B* **6**, 459
- N. Andersen and P. Sigmund, 1974: *Mat. Fys. Medd. Dan. Vid. Selsk.* **39** no. 3
- J. P. Biersack and W. Eckstein, 1984: *Appl. Phys. A* **34**, 73
- L. Boltzmann, 1875: *Sitzungsber. Akad. Wiss. Wien, Math. Naturwiss. Kl.* **72**, 427
- J. J. Duderstadt and W. R. Martin, 1979: *Transport Theory*, Wiley, New York
- L. G. Glazov, 1994a: *J. Phys. Cond. Matt.* , **6**, 4181
- L. G. Glazov, 1994b: *J. Phys. Cond. Matt.* **6**, 10647
- L. G. Glazov, 1995: *J. Phys. Cond. Matt.* **7**, 6365
- D. E. Harrison and M. M. Jakas, 1984: *Phys. Rev. B* **30**, 3573
- D. E. Harrison and M. M. Jakas, 1985: **32**, 2753
- M. Hautala and H. J. Whitlow, 1985: *Nucl. Instrum. Methods B* **6**, 466
- W. Huang, H. M. Urbassek, and P. Sigmund, 1985: *Phil. Mag.* **52**, 753
- R. E. Johnson and J. Schou, 1993: *Mat. Fys. Medd. Dan. Vid. Selsk.* **43**, 403
- K. Kopitzki and H. E. Stier, 1961: *Z. Naturforsch.* **16a**, 1257
- K. Kopitzki and H. E. Stier, 1962: *Z. Naturforsch.* **17a**, 346
- J. Lindhard and V. Nielsen, 1971: *Mat. Fys. Medd. Dan. Vid. Selsk.* **38** no. 9
- J. Lindhard, V. Nielsen, M. Scharff, and P. V. Thomsen, 1963a: *Mat. Fys. Medd. Dan. Vid. Selsk.* **33** no. 10
- J. Lindhard, M. Scharff, and H. E. Schiøtt, 1963b: *Mat. Fys. Medd. Dan. Vid. Selsk.* **33** no. 14
- J. Lindhard, V. Nielsen, and M. Scharff, 1968: *Mat. Fys. Medd. Dan. Vid. Selsk.* **36** no. 10
- U. Littmark, 1974: Thesis, Univ. Copenhagen
- U. Littmark and W. O. Hofer, 1980: *Nucl. Instrum. Methods B* **168**, 329
- U. Littmark and P. Sigmund, 1975: *J. Phys. D* **8**, 241
- N. Matsunami, Y. Yamamura, Y. Itikawa, N. Itoh, Y. Kazumata, S. Miyagawa, K. Morita, R. Shimizu, H. Tawara, 1984: *At. Data & Nucl. Data Tab.* **31**, 1
- C. T. Reimann, 1993: *Mat. Fys. Medd. Dan. Vid. Selsk.* **43**, 351
- M. T. Robinson, 1965: *Phil. Mag.* **12**, 741
- H. Roosendaal and J. B. Sanders, 1980: *Radiat. Eff.* **52**, 137; *Proceedings of the Symposium on Sputtering*, edited by P. Varga et al., *Inst. Allg. Phys. Wien*, 302

- H. E. Roosendaal, J. B. Sanders, & U. Littmark, 1982: Phys. Rev. B **26**, 5261
- J. B. Sanders, 1968: Thesis, Univ. Leiden
- L. I. Schiff, 1981: *Quantum Mechanics*, 3rd edition, McGraw-Hill, Auckland etc.
- M. W. Sckerl, M. Vicanek, and P. Sigmund, 1995: Nucl. Instrum. Methods B **102**, 86
- M. H. Shapiro, P. K. Haff, T. A. Tombrello, and D. E. Harrison, 1985: Nucl. Instrum. Methods B **12**, 137
- M. H. Shapiro, T. A. Tombrello, and D. E. Harrison, 1988: Nucl. Instrum. Methods B **30**, 152
- V. I. Shulga and P. Sigmund, 1995: Nucl. Instrum. Methods B **103**, 383
- V. I. Shulga and P. Sigmund, 1996: Submitted to Nucl. Instrum. Methods B
- P. Sigmund, 1968: Can. J. Phys. **46**, 731
- P. Sigmund, 1969a: Appl. Phys. Lett. **14**, 114
- P. Sigmund, 1969b: Phys. Rev. **184**, 383; **187**, 768
- P. Sigmund, 1969c: Radiat. Eff. **1**, 15
- P. Sigmund, 1972: Rev. Roum. Phys. **17**, 823; 969; 1079
- P. Sigmund, 1973: Unpublished
- P. Sigmund, 1981: in *Sputtering by Particle Bombardment I*, edited by R. Behrisch, Top. Appl. Phys. (Springer) **47**, 9
- P. Sigmund, 1991: in *Interaction of Charged Particles with Solids and Surfaces*, edited by A. Gras-Marti et al., NATO ASI Series Vol. **271**, 73
- P. Sigmund and A. Gras-Marti, 1981: Nucl. Instrum. Methods **182/183**, 25
- P. Sigmund and N. Q. Lam, 1993: Mat. Fys. Medd. Dan. Vid. Selsk. **43**, 255
- P. Sigmund and M. W. Sckerl, 1993: Nucl. Instrum. Methods B **82**, 242
- M. W. Thompson, 1968: Phil. Mag. **18** 377
- H. M. Urbassek and M. Vicanek, 1988: Phys. Rev. B **37**, 7256
- H. M. Urbassek and M. Vicanek, 1992: Unpublished
- H. M. Urbassek, G. Mayer, H. Gades, and M. Vicanek, 1995: Nucl. Instrum. Methods B **103**, 275
- M. Vicanek, U. Conrad, and H. M. Urbassek, 1993: Phys. Rev. B **47**, 617
- M. Vicanek and H. M. Urbassek, 1988: Nucl. Instrum. Methods B **30**, 507
- K. T. Waldeer and H. M. Urbassek, 1987: Nucl. Instrum. Methods B **18**, 518
- K. T. Waldeer and H. M. Urbassek, 1988: Appl. Phys. A **45**, 207
- K. B. Winterbon and P. Sigmund, 1973: Unpublished
- K. B. Winterbon, P. Sigmund, and J. B. Sanders, 1970: Mat. Fys. Medd. Dan. Vid. Selsk. **37** no. 14

Submitted to the Academy December 1995

Published March 1996

